Effect of wall heating on turbulent boundary layers with temperature-dependent viscosity

Jin Lee[1,2], Seo Yoon Jung[1], Hyung Jin Sung[2] and Tamer A. Zaki[1],†

[1]Department of Mechanical Engineering, Imperial College London, South Kensington Campus, London SW7 2AZ, UK

[2]Department of Mechanical Engineering, KAIST, 291 Daehak-ro, Yuseong-gu, Daejeon, 305-701, Korea

Direct numerical simulations (DNS) of turbulent boundary layers over isothermally heated walls were performed, and the effect of viscosity stratification on the turbulence statistics and skin friction were investigated. An empirical relation for temperature-dependent viscosity for water was adopted. Based on the free-stream temperature (30°C), two wall temperatures (70°C and 99°C) were selected. In the heated flows, the turbulence energy diminishes in the buffer layer, but increases near the wall. The reduction in turbulence kinetic energy in the buffer layer is accompanied by smaller levels of Reynolds shear stresses and, hence, weaker turbulence production. The enhanced turbulence energy near the wall is attributed to enhanced transfer of energy via additional diffusion-like terms due to the viscosity stratification. Despite the lower fluid viscosity near the wall, dissipation is also increased owing to the augmented near-wall fine-scale motion. Wall heating results in reduction in the skin-friction coefficient by up to 26 %. An evaluation of the different contributions to the skin friction demonstrates that drag reduction is primarily due to the changes in the Reynolds shear stresses across the boundary layer. Quadrant and octant analyses showed that ejections (Q2) and sweeps (Q4) are significantly reduced, a result further supported by an examination of outer vortical structures from linear stochastic estimation of the ejection events and spanwise vortices.

Key words: turbulent boundary layers, turbulent flows

---

1. Introduction

There is considerable interest in the reduction of skin friction in turbulent boundary layers (TBL) of liquid flows. In general, skin-friction reduction can be achieved by a change of fluid characteristics or via morphological features (Bushnell & Moore 1991). One example of the former approach is introducing a gas layer with a lower kinematic viscosity near the wall (Ceccio 2010). For water flows, the reduction of fluid viscosity can also be readily achieved by wall heating, since the viscosity of common liquids decreases with increasing temperature. However, the effects of the gradual change of the viscosity, i.e. viscosity stratification, on boundary layer turbulence and in turn on drag are not clear. Therefore, the present study aims to examine the mechanics of skin-friction and turbulence modification in response to wall heating of turbulent boundary layers with temperature-dependent viscosity.

† Email address for correspondence: t.zaki@imperial.ac.uk

Several studies have investigated the effect of wall heating on the linear stability of laminar shear flows with temperature-dependent viscosity. Wall & Wilson (1996, 1997) examined the instability of channel and boundary layer flows. They attributed the changes in the flow instabilities to three physical effects: the bulk, the velocity profile and the thin-layer effects. Among these, the thin-layer effect was most critical for stability of the laminar base state. More recently, Sameen & Govindarajan (2007) examined transient disturbances in laminar channel flow. The linear analyses predict that heating has a stabilizing influence on liquid flows, and thus provides a possible strategy for transition delay. Experimental evidence includes the work of Lauchle & Gurney (1984) who examined axisymmetric boundary layers over an underwater body, and found that the laminar–turbulence transition was significantly delayed to higher Reynolds numbers when the body was heated. In the context of direct numerical simulations (DNS), Kral & Fasel (1994) investigated the effect of passive control using wall heating on the transition process. They found that the amplitudes and growth rates of instability waves were significantly reduced for uniform wall heating.

While the above studies have addressed the influence of heating on transition, the influence on fully turbulent flows, for example turbulent skin friction and flow structures, remains unknown. One exception is the recent work of Zonta, Marchioli & Soldati (2012) who performed DNS of heated turbulent channel flow. They examined the effect of inhomogeneous viscosity and found that turbulence production and dissipation of the wall-bounded flow were dramatically changed. Their work, however, did not consider heating of spatially developing flows.

A number of studies in the literature have been devoted to numerical simulations of turbulent thermal shear flows including, for example, the work of Kong, Choi & Lee (2000) and Li (2011). These efforts have focused on scalar transport, and contributed to our understanding of turbulence structures of the velocity and temperature fluctuations in flows with various thermal boundary conditions and at different Prandtl numbers. Based on their DNS of turbulent thermal boundary layers, Kong *et al.* (2000) demonstrated the similarity between wall-normal heat flux and the Reynolds stresses, which underlies the correlation between the temperature and the streamwise velocity perturbation fields. In addition, previous simulations have demonstrated that the scalar fluctuations and the scalar flux were increased with increasing Prandtl number. These studies have assumed constant fluid properties, in particular the fluid viscosity, or equivalently the Prandtl number. We herein relax this assumption and consider the case of temperature-dependent viscosity, where the Prandtl number varies spatially within the thermal boundary layer.

The analysis of the effect of heating on turbulent skin friction builds on previous efforts in the field of turbulent-flow control. Numerous mechanisms have been suggested based on a comprehensive study of turbulent structures. For example, modulation of the near-wall streamwise vortices which contribute appreciably to the skin friction has been proposed. Choi, Moin & Kim (1994) used an active control strategy to cancel out streamwise vortices. In their work, vertical and spanwise velocities near the wall were controlled with actuators at the wall. However, this concept requires an abundance of sensors and actuators to manipulate the near-wall vortices. Choi, Moin & Kim (1993) employed a riblet surface for the passive control of turbulent channel flow and found that small spacings of the riblets ($s^+ \approx 20$) reduce the friction drag by disturbing the location of the streamwise vortices. Although this
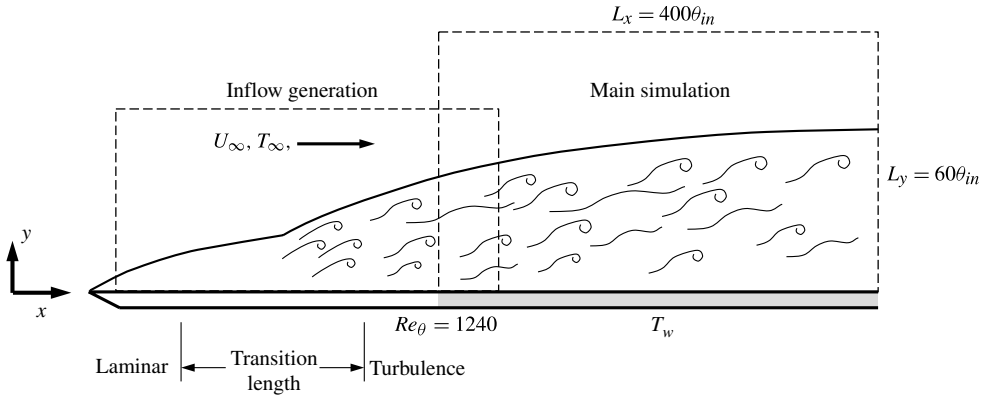
FIGURE 1. Computational domain and coordinate system. Spanwise (z) direction is outward from the figure. Grey area is isothermal heated wall.

method can be more easily realized than an active control strategy, an important consideration is that the minimum spacing for drag reduction depends on Reynolds number.

Other strategies for drag reduction include injection of low-viscosity fluid for underwater bodies (Ceccio 2010) and surface treatment for free-slip walls (Min & Kim 2004). The former case is difficult to maintain, since the outer fluid sweeps the injected low-viscosity fluid away from the surface. In the case of hydrophobic surface treatment, ongoing research continues to target the necessary large slip length (Min & Kim 2004). Exploration of practical methods for the reduction of friction drag in turbulent boundary layers is of great importance (Bushnell & Moore 1991), and strategies which are easy to implement and have wide applicability are particularly desirable.

The purpose of the current study is to investigate the influence of viscosity stratification by wall heating on skin-friction reduction in turbulent boundary layers. To this end, DNS are performed to examine forced convection in TBLs with temperature-dependent viscosity. A schematic diagram of the computational domain is shown in figure 1. Two values of the wall temperature, $T_w = 70°C$ and $99°C$, which represent moderately heated (MH) and strongly heated (SH) walls, are considered. Note that the minimum viscosity above the heated wall is 50 % of the free-stream value for the MH case and 35 % for the SH case. The influence of wall heating on skin friction and turbulence structures is examined in detail. For comparison, an isothermal configuration ($T_\infty = T_w = 30°C$), herein referred to as an unheated wall (UH), was also simulated. A passive scalar was included in the UH flow in order to model the scalar (or temperature) field in the case of constant fluid properties.

This paper is organized in six sections. Section 2 includes the numerical method and the viscosity model adopted in this work. Section 3 demonstrates the influence of heating on the skin friction, the mean flow and the turbulence statistics. The remaining sections aim to explain these effects from various angles. Section 4 focuses on the changes to terms in the turbulent kinetic energy budget, and § 5 discusses the turbulent flow structures, and the underlying mechanism of skin-friction reduction. Finally, a summary of the present study is presented in the last section.

2. Numerical methods

In this study, the temperature-dependent viscosity of the fluid is defined according to the 'Arrhenius-type' viscosity model for water (White 2006):

$$\ln\left(\frac{\mu}{\mu_{ref}}\right) = a + b\left(\frac{T_{ref}}{T}\right) + c\left(\frac{T_{ref}}{T}\right)^2,$$ (2.1)

where the curve-fit values are $a = -2.10$, $b = -4.45$ and $c = 6.55$ corresponding to $T_{ref} = 273$ K and $\mu_{ref} = 0.00179$ kg m^{-1} s^{-1}. In order to isolate the effect of wall heating on viscosity variation alone, other thermal properties including density (ρ) and thermal diffusivity (α) were assumed to be constant as set by the free-stream temperature. This assumption is appropriate for most common liquids, such as water, since changes in viscosity are much more significant than changes in density and in thermal diffusivity (Incropera & Dewitt 1985). Over the range of temperatures considered, the normalized change in water viscosity is $\Delta\mu/\mu \simeq 65\%$, while for the density $\Delta\rho/\rho \leqslant 3.7\%$. In effect, the current simulations address the forced convection problem, when the ratio of the Grashof number to the square of the Reynolds number is small, $Gr/Re^2 \ll 1$. A similar assumption has been invoked previously by several numerical studies (Kral & Fasel 1994; Wall & Wilson 1996, 1997; Sameen & Govindarajan 2007; Zonta *et al.* 2012), which investigated the effect of temperature-dependent viscosity.

The continuity, the Navier–Stokes and the energy equations for an incompressible flow with temperature-dependent viscosity are written as:

$$\frac{\partial u_i}{\partial x_i} = 0,$$ (2.2)

$$\frac{\partial u_i}{\partial t} + u_j\frac{\partial u_i}{\partial x_j} = -\frac{\partial p}{\partial x_i} + \frac{1}{Re_{\theta_{in}}}\frac{\partial}{\partial x_j}\left[\nu_R\left(\frac{\partial u_i}{\partial x_j} + \frac{\partial u_j}{\partial x_i}\right)\right],$$ (2.3)

$$\frac{\partial \Theta}{\partial t} + u_j\frac{\partial \Theta}{\partial x_j} = \frac{1}{Re_{\theta_{in}}Pr}\frac{\partial^2 \Theta}{\partial x_j^2}.$$ (2.4)

The velocity components in the streamwise (x), wall-normal (y) and spanwise (z) directions are u, v and w, respectively, and the kinematic pressure is p. The non-dimensionalized temperature is defined as $\Theta = (T - T_w)/(T_\infty - T_w)$. Here, subscripts w and ∞ denote variables at the wall and in the free stream, respectively. Hereafter, uppercase symbols (except the temperature) refer to mean quantities and primed symbols, such as u', are reserved for fluctuations. The free-stream velocity U_∞ and the momentum thickness at the inlet θ_{in} are chosen as the reference velocity and length scales. The viscosity ratio ν_R is the ratio of the local to the free-stream viscosity, $\nu(T)/\nu_\infty$. Since density is assumed to be constant, the kinematic viscosity is simply $\mu(T) = \rho\nu(T)$. The Reynolds number and Prandtl number in the governing equations are $Re_{\theta_{in}}(\equiv U_\infty\theta_{in}/\nu_\infty) = 1240$ and $Pr(\equiv \nu_\infty/\alpha) = 5.4$, respectively. Here, α is the thermal diffusivity.

The Navier–Stokes equations were solved using a fractional step algorithm on a staggered grid with a local volume-flux formulation (Rosenfeld, Kwak & Vinokur 1991). The viscous terms were integrated in time implicitly using the Crank–Nicolson method and the convective terms were treated explicitly using the Adams–Bashforth scheme. The pressure term was discretized by an implicit Euler scheme. This algorithm was previously used in DNS of transitional and turbulent boundary layer flows (e.g. Zaki *et al.* 2010). For the energy equation, the same time integration and

	T_w [°C]	T_∞ [°C]	$\nu_R\|_w$	$L_x \times L_y \times L_z$ [$\theta_{in} \times \theta_{in} \times \theta_{in}$]	Number of grid points	Δt [θ_{in}/U_∞]
Strongly heated (SH)	99	30	0.352	$400 \times 60 \times 80$	$4097 \times 385 \times 1281$	0.015
Moderately heated (MH)	70	30	0.497	$400 \times 60 \times 80$	$4097 \times 385 \times 1281$	0.018
Unheated (UH)	30	30	1.000	$400 \times 60 \times 80$	$4097 \times 385 \times 1281$	0.025

TABLE 1. Parameters of the DNS.

spatial discretization as those for the Navier–Stokes equations were adopted, except for the nonlinear term. In order to represent the sharp gradients in temperature, a fifth-order upstream central scheme (Nourgaliev & Theofanous 2007) was employed for the convective term of the energy equation.

Spatially developing turbulent flows are challenging to simulate numerically due to their spatial inhomogeneity and the requirement to prescribe a time-dependent, turbulent inflow condition. In order to generate a realistic inflow for the main simulations, a precursor simulation of a transitional boundary layer was performed (see figure 1). The setup of the auxiliary computation is similar to the simulations by Jacobs & Durbin (2001): isotropic free-stream turbulence was used at the inlet in order to trigger breakdown of a laminar boundary layer to turbulence. The free-stream turbulence intensity was 3 % at the inlet, and inappreciable (less than 0.5 %) in the fully turbulent regime. The domain length spanned the region $106 \leqslant Re_\theta \leqslant 1400$ which overlaps with the main simulation domain. Boundary layer transition took place at $Re_\theta = 280$. Instantaneous y–z flow data were extracted sufficiently far downstream, at $Re_\theta = 1240$. The time series was subsequently applied as inflow condition in the main simulation.

The parameters of the main simulation are summarized in table 1. The size of the computational domain is $L_x = 400\theta_{in}$, $L_y = 60\theta_{in}$ and $L_z = 80\theta_{in}$. Isothermal heating is applied downstream of the inlet. At the end of the streamwise domain, the Reynolds number of the unheated case reaches $Re_\theta = 2060$, and the wall-normal extent of the domain is approximately five times the boundary layer thickness at the exit. The spanwise extent is sufficiently large to avoid spanwise correlation. The grid spacing of the present study is sufficient to resolve the smaller Kolmogorov microscale in the case of wall heating (see table 2). Moreover, in terms of the smallest spatial scale of the temperature field η_θ, the maximum grid spacing (table 3) is comparable to that used by Zonta *et al.* (2012), i.e. $(\Delta x/\eta_\theta)_{max} = 12$, $(\Delta y/\eta_\theta)_{max} = 2$ and $(\Delta z/\eta_\theta)_{max} = 6$ in their study. A non-uniform grid distribution is used in the wall-normal direction, whereas uniform grid spacing was used in the streamwise and the spanwise directions. The computational time step was $\Delta t = \{0.025, 0.018, 0.015\}\theta_{in}/U_\infty$ for the UH, MH and SH cases, respectively, and the total averaging time was $1800\theta_{in}/U_\infty$. The simulations were carried out using 2048 cores on HECToR Phase 3 (Cray XE6, Interlagos).

The convective outflow condition $\partial u_i/\partial t + c\partial u_i/\partial x = 0$ was applied at the outlet of the main simulation, where c is the local bulk velocity. The no-slip condition was imposed at the bottom wall. Periodic boundary conditions were applied in the spanwise direction. At the top of the computational domain, the streamwise velocity was prescribed, $u = U_\infty$, and the wall-normal velocity was evaluated from the continuity equation, $v = -(\mathrm{d}/\mathrm{d}x) \int_0^{L_y} u \, \mathrm{d}y$.

	Δx^+	Δy^+_{min}	Δy^+_{max}	Δz^+	Δt^+
Strongly heated (SH)	12.2	0.593	21.1	7.82	0.0698
Moderately heated (MH)	9.22	0.447	22.4	5.90	0.0670
Unheated (UH)	5.08	0.246	24.6	3.25	0.0564

TABLE 2. Spatial and temporal resolution.

	$(\Delta x/\eta_\theta)_{max}$	$(\Delta y_{min}/\eta_\theta)_{max}$	$(\Delta y_\delta/\eta_\theta)_{max}$	$(\Delta z/\eta_\theta)_{max}$
Strongly heated (SH)	12.4	0.599	2.98	7.91
Moderately heated (MH)	11.0	0.531	3.01	7.01
Unheated (UH)	8.3	0.402	3.04	5.31

TABLE 3. Maximum spatial resolution normalized by the smallest spatial scale of the temperature field η_θ, which is defined as $\eta_\theta \equiv \eta\sqrt{1/Pr}$ (Zonta *et al.* 2012). Subscript δ denotes value at the edge of the momentum boundary layer.

In order to ascertain the reliability and accuracy of these numerical simulations, the velocity statistics for the unheated case ($T_w = T_\infty$) are compared to the experimental data of Purtell, Klebanoff & Buckley (1981) and the numerical data of Wu & Moin (2010). Good agreement with these datasets is demonstrated in figure 2. In the same figure, the mean scalar profile is compared to the correlation by Kader (1981) for boundary layers, and shows favourable agreement. In addition, both the mean and the root-mean-square (r.m.s.) of the scalar are compared to the numerical simulations by Kawamura *et al.* (1998) for channel flow since data are not available for turbulent boundary layers at the same Prandtl number. Profiles of the heated flows have not been compared with either experimental or computational results, since no dataset is available for the present flow configuration. Further discussion of the mean streamwise velocity and the Reynolds stresses is presented in § 3.1.

3. Mean flow statistics

This section discusses the effect of wall heating for a liquid with temperature-dependent viscosity on the turbulence statistics and the skin-friction coefficient. As mentioned in § 1, numerous studies have shown that wall heating stabilizes wall-bounded liquid flows and delays transition to turbulence. However, reduction of skin friction in the turbulent regime has not been examined previously. First, the drag reduction rate is quantified based on the skin-friction coefficient. Next, the mean streamwise velocity and Reynolds stresses of the heated flows are compared with those of the unheated case. Finally, the three physical effects relevant to viscosity stratification, and noted by Wall & Wilson (1997), are evaluated for the present flow fields.

3.1. *Skin friction and turbulent statistics*

The skin-friction coefficient C_f is shown in figure 3(*a*) as a function of Re^{eff}_θ. Here, the effective Reynolds number Re^{eff}_θ is defined as

$$Re^{eff}_\theta \equiv \frac{U_\infty\theta}{\nu^{eff}}, \qquad (3.1)$$
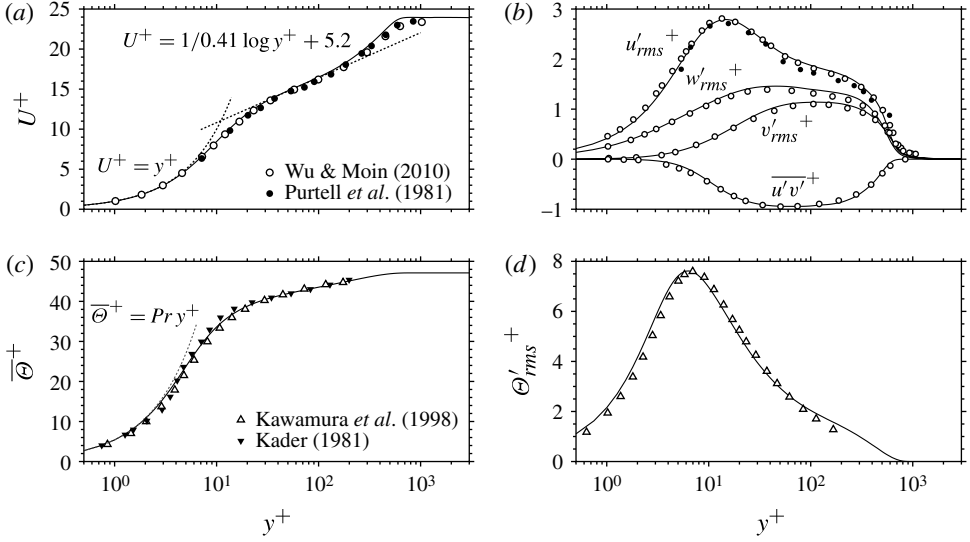
FIGURE 2. Turbulence statistics of the unheated case ($T_w = T_\infty$) at $Re_\theta = 1840$. (a) The mean streamwise velocity; (b) r.m.s. of turbulence intensities and the Reynolds shear stress normalized by u_τ. (c) Mean scalar and (d) r.m.s. of scalar fluctuation. Profiles in (c,d) are normalized by the friction temperature.
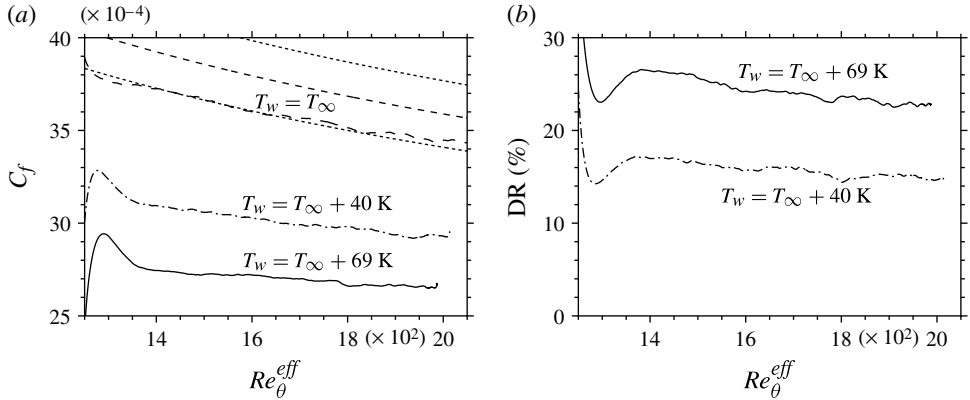

FIGURE 3. (a) Skin-friction coefficient as a function of the effective Reynolds number. Dashed line represents the correlation $C_f = 0.024 Re_\theta^{-1/4}$ by Smits *et al.* (1983) and dotted lines to each side of it represent a 5 % tolerance. (b) Drag reduction rate (DR = ($C_f(T_w = T_\infty) - C_f)/C_f(T_w = T_\infty)$) as function of the effective Reynolds number.

where ν^{eff} is given by

$$\nu^{eff} \equiv \frac{1}{\delta} \int_0^\delta \bar{\nu}(y) \, dy. \tag{3.2}$$

First, the range of Re_θ^{eff} is slightly decreased for the heated flows despite the same length of the computational domain. This is due to a reduction in the momentum

thickness, θ, which is discussed in §3.2. It is clearly seen in figure 3(a) that the skin friction of the temperature-dependent-viscosity fluids is reduced by wall heating. The reduction in C_f is more pronounced for the SH case. Note that C_f of the UH case is within a 5% tolerance of the correlation by Smits, Matheson & Joubert (1983). As shown in figure 3(b), C_f of the heated flows is significantly reduced just downstream of the inlet ($Re_\theta^{eff} = 1240$), where wall heating starts. Since the increased wall temperature leads to lower viscosity at the wall (see table 1), it directly affects the decrease in C_f. However C_f recovers as the flow develops downstream, and forms a local maximum at $Re \approx 1280$. The rapid increase of C_f results from the increase in the mean shear rate $\partial U/\partial y$ in the near-wall, low-viscosity region. After the peak, C_f decreases by approximately 17% and 26% of the reference value at $Re_\theta^{eff} = 1410$ for the MH and SH cases, respectively. Farther downstream, at $Re_\theta^{eff} = 1840$, the drag reduction rate is approximately 15% and 23% for the MH and SH cases. This suggests that wall heating is a viable skin-friction reduction strategy for fully turbulent flows. Furthermore, it should be noted that the skin friction is reduced over the entire Re range. Even though the drag reduction rate slightly decreases as Re increases, it still shows that the temperature stratification results in significant reduction in the skin friction. Hereinafter, many of the results will be plotted at $Re_\theta^{eff} = 1840$. This location is sufficiently downstream in order to eliminate the effect of the sudden heating at the inlet to the domain, and is sufficiently upstream of the exit plane to avoid contamination by the outflow boundary condition. In addition, this Reynolds number corresponds to existing data in the literature (e.g. Wu & Moin 2010) which have been used for validation of the isothermal, reference case.

For the purpose of the discussion of the turbulence statistics, an appropriate inner length scale must be defined. In isothermal flows, the inner length scale is generally chosen as $l = \nu/u_\tau$, which is the ratio of kinematic viscosity to the friction velocity $u_\tau(=\sqrt{\tau_w/\rho_w})$, and is only a function of the streamwise location. It is evident that appropriate definition of the inner length scale is desirable for flows with inhomogeneous viscosity. In the present case, viscosity is not a function of the streamwise location only, but also of the wall-normal distance. Hence, we adopt the modified inner length scale, $l_\nu = \bar{\nu}(x, y)/u_\tau$, based on the local mean viscosity $\bar{\nu}(y)$ and the wall friction velocity. Note that the overbar denotes a time-averaged quantity. The modified length scale is shown in figure 4. Whereas the length scale of the isothermal flow is constant, that of the heated flows decreases near the wall and increases away from the wall. Near the boundary layer edge ($y/\delta = 1$), the local viscosity is identical among all cases due to the thin thermal boundary layer thickness at high Pr. Nevertheless, the length scale is increased for the heated flows because the friction velocity is reduced. Near the wall ($y/\delta < 0.1$), the modified length scale of the heated flows decreases due to the small local viscosity. Using a similar argument, Huang, Coleman & Bradshaw (1995) introduced $y^*(=y\sqrt{(\tau_w/\bar{\rho}(y))}/\bar{\nu}(y))$ for compressible channel flow and found that use of y^* (which is based on τ_w and local thermal properties) is more advantageous for the wall coordinate than use of either wall properties or averaged properties in the cross-stream plane. The present wall-normal coordinate normalized by the inner length scale $y_\nu^+ = y/l_\nu$ is essentially the same as y^* of Huang $et~al.$ (1995), since density is constant in the present study. Hereafter, all results based on inner scales will be plotted using the modified length scale.

The mean streamwise velocity normalized by U_∞ is shown in figure 5(a), at $x/\theta_{in} = 275$. At the same physical location, the mean velocity increases below $y/\delta \approx 0.4$
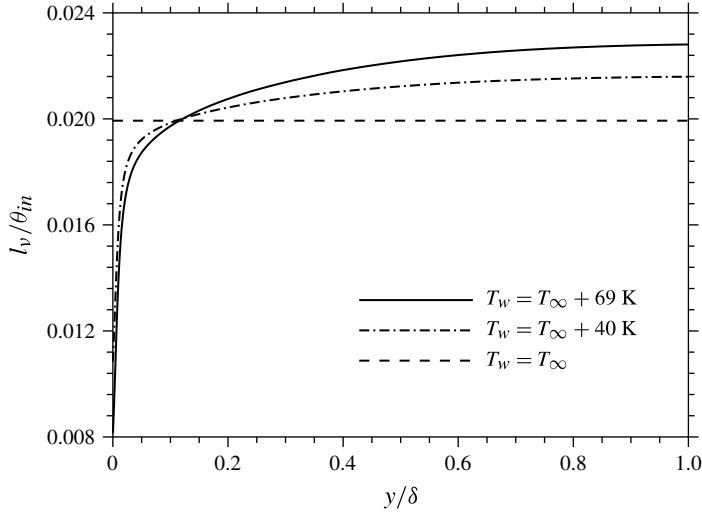
FIGURE 4. Profiles of the modified inner-length scale (l_v) at $x/\theta_{in} = 275(Re_\theta = 1840$ for $T_w = T_\infty)$.
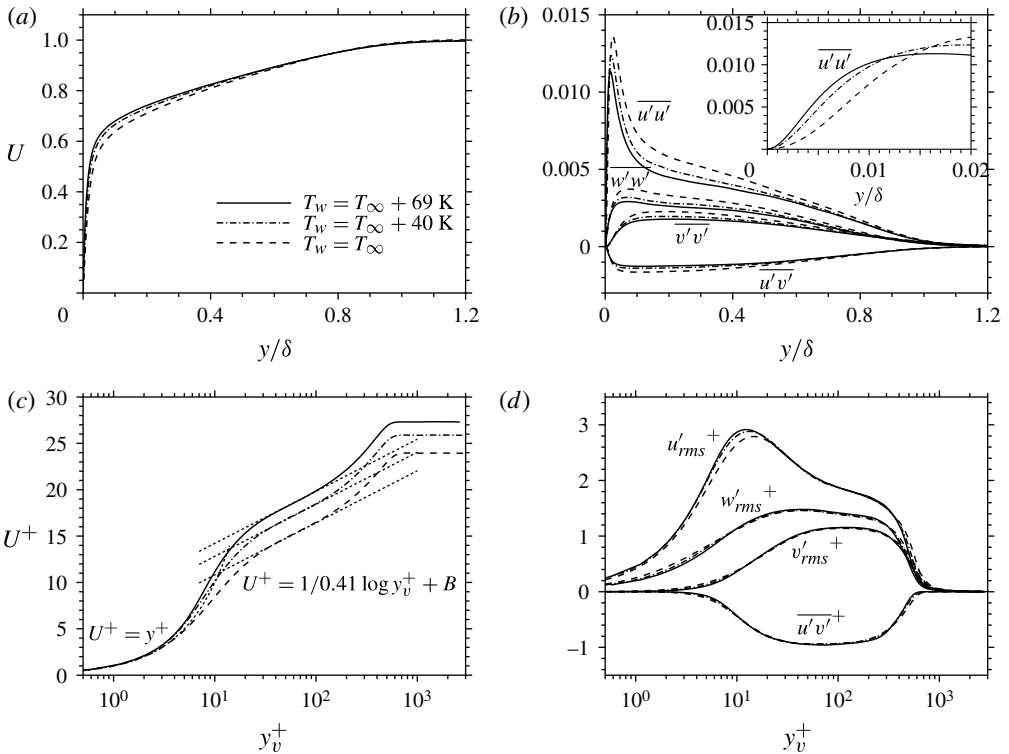

FIGURE 5. Profiles of: (*a*) the mean streamwise velocity normalized by U_∞ and (*b*) variance of turbulence intensities and the Reynolds shear stress normalized by U_∞^2; (*c*) the mean streamwise velocity and (*d*) r.m.s. of velocity fluctuations and the Reynolds shear stress normalized by u_τ. All profiles are drawn at $x/\theta_{in} = 275(Re_\theta = 1840$ for $T_w = T_\infty)$.

as wall temperature increases. Near the boundary layer edge, the velocity is almost identical in all cases. This is qualitatively consistent with previous studies which describe an increase of the laminar base-flow velocity profile near the heated wall (Wall & Wilson 1996, 1997; Sameen & Govindarajan 2007). Turbulence intensities and Reynolds shear stress normalized by U_∞^2 are shown in figure 5(b). As the wall temperature increases, all components of the turbulence intensity decrease from the buffer layer, where the peak of $\overline{u'u'}$ is located, to the boundary layer edge. The wall-normal location of the peak position moves towards the wall. The trend of weaker turbulent fluctuations prevails in all the velocity components and in the Reynolds shear stress. However, as shown in the inset of figure 5(b), $\overline{u'u'}$ is increased in the near-wall region. This results from the downward shift of the peak position. The decreased Reynolds stresses are qualitatively consistent with those in the turbulent channel flows with variable viscosity: Zonta *et al.* (2012) mentioned that the decreased turbulence intensities result from a stabilizing effect of the low viscosity near the heated wall.

The mean streamwise velocity is shown in figure 5(c) normalized by u_τ. The standard law of the wall is also plotted in the figure. In the log-layer, when the wall is heated, the profiles are shifted upward from the unheated state with the same inclination angle. The intercept B increases from 5.2 (UH) to 7.2 (MH) and 8.6 (SH), while the von Kármán constant ($\kappa = 0.41$) is identical. Although the universality of the value of κ remains the subject of active research (Nagib & Chauhan 2008; Marusic *et al.* 2010), in the current simulations, the slope of the log-layer remains unchanged irrespective of the wall temperature. The upward shift in the velocity profile has been observed in previous studies of flows with reduced skin friction (Choi *et al.* 1993, 1994; Min & Kim 2004). The thickness of the log-layer where the log-law is satisfied is almost unchanged in all cases. However, the thickness of the sublayer where the linear law is satisfied is decreased from 5.92 (UH) to 2.28 (MH) and 2.19 (SH) in wall units, with increasing wall temperature. Figure 5(d) shows the r.m.s. of the velocity fluctuations and the Reynolds shear stress. Although these quantities decreased based on outer scaling (figure 5b), they show better agreement regardless of the wall temperature when normalized by u_τ. The agreement demonstrates that the modified inner length scale is the appropriate scaling.

The choice of suitable reference scales depends on the objective of the investigation. For example, if one wishes to examine the influence of viscosity variations on the turbulence dynamics, then the appropriate scales are the local friction velocity and the modified length scale $l_\nu = \bar{\nu}(x, y)/u_\tau$, as demonstrated above. On the other hand, in the current study, the aim is to assess the impact of wall heating on the turbulent boundary layer flow, in comparison to the unheated case. The simulation setup assumes that heating starts downstream of the inlet plane, and therefore the inflow condition is identical among all cases. In order to determine the changes due to wall heating, relative to the unheated case, the inflow U_∞ and θ_{in} are adopted as the reference scales hereafter. These are common among all the simulations, and therefore allow a direct comparison between the unheated and heated flows.

The mean scalar profiles are shown in figure 6(a) normalized by the friction temperature, $\Theta_\tau \equiv -(\alpha/u_\tau)(\partial\overline{\Theta}/\partial y)_w$. The wall-normal position on the abscissa is normalized by the modified inner length scale. The modified linear law for the mean scalar, which is defined by $\overline{\Theta}^+ = Pr(y)y_\nu^+$, is also plotted in the figure. Note that Pr is dependent on the wall-normal distance due to viscosity stratification, unlike previous studies of passive scalar transport in isothermal turbulent boundary layers. Thus, as the fluid temperature is increased due to proximity to the heated wall, $Pr(y)$ is decreased and the mean scalar is reduced. In addition, the mean scalar profile is
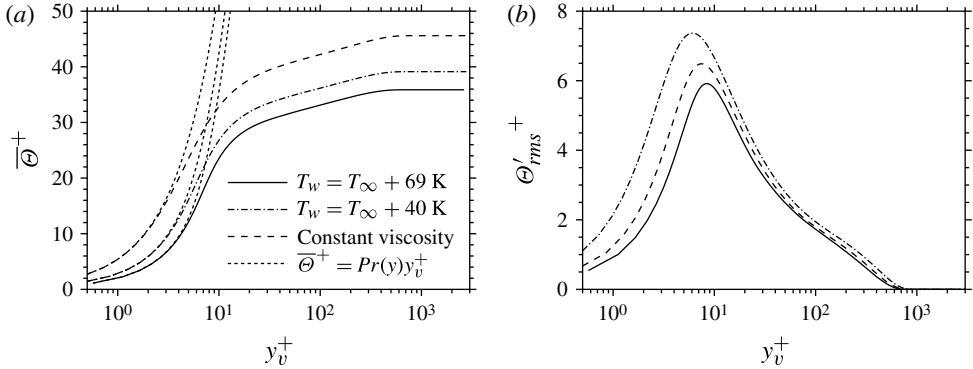
FIGURE 6. Wall-normal distribution of (*a*) mean scalar and (*b*) r.m.s. of scalar fluctuation at $x/\theta_{in} = 275 (Re_\theta = 1840$ for $T_w = T_\infty)$. Each profile is normalized by the friction temperature.

decreased throughout the boundary layer due to the higher friction temperature (Li 2011). This accounts for the lower scalar profile in the wake region for the heated flows, even though $Pr(y)$ has reached the reference value. The r.m.s. of the scalar fluctuation is shown in figure 6(*b*). Similarly to the mean scalar profile, increasing the wall temperature results in a decrease in the r.m.s. of the scalar fluctuations.

In this subsection, reduction of C_f with wall heating has been introduced. In the Re range considered, the skin friction was reduced to three-quarters of the reference value for the strongly heated flow. It was also shown that the streamwise velocity is increased near the heated walls, and that all the Reynolds stresses are weakened in the outer region. The following subsections provide an evaluation of three mechanisms that can result from viscosity stratification, in order to determine the most likely influence. These mechanisms as described by Wall & Wilson (1997) are the bulk effect, the velocity profile and the thin-layer effect.

3.2. *The bulk effect*

The bulk effect refers to changes in the boundary layer flow due to the effective Reynolds number, which depends on the effective viscosity. The latter is defined as the average viscosity ratio inside the momentum boundary layer (see (3.2)). Figure 7(*a*) shows the downstream variation in ν_R^{eff}. Whereas the viscosity ratio in the vicinity of the wall drops significantly, the effective value is only reduced by approximately 2 % (MH) and 3 % (SH), respectively. Figure 7(*a*) also shows the displacement (δ^*) and momentum (θ) thicknesses along the streamwise direction. As a general trend, as the wall temperature increases, the growth rate of both thicknesses becomes smaller than that of the UH case. It should be noted, however, that the hydrodynamic boundary layer thickness (δ; not shown) is nearly independent of the wall temperature. The reason can be inferred from the streamwise velocity profile: while the flow is accelerated near the wall, the streamwise velocity is unchanged near the edge of the boundary layer (figure 5*a*).

The effective Reynolds number Re_θ^{eff} is plotted in figure 7(*b*). In the presence of wall heating, Re_θ^{eff} is only slightly decreased. Overall the bulk effect remains inappreciable and is therefore not expected to be a leading cause of the observed reduction in skin friction.
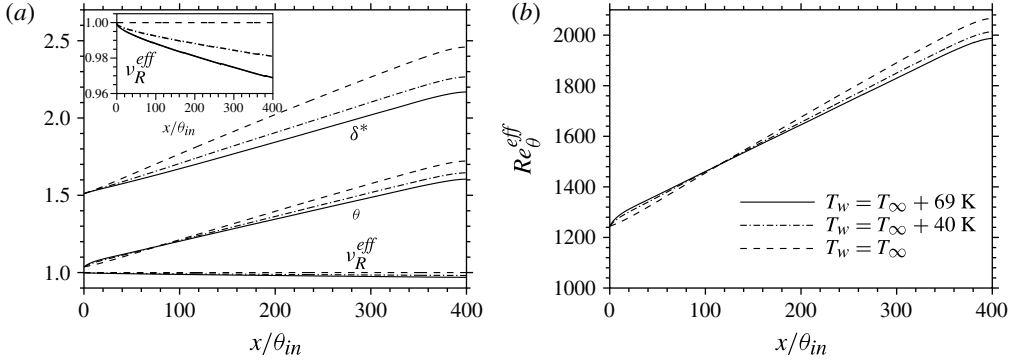
FIGURE 7. Streamwise variation of (*a*) displacement thickness (δ^*), momentum thickness (θ) and effective viscosity ratio and (*b*) effective Reynolds number (Re_θ^{eff}).
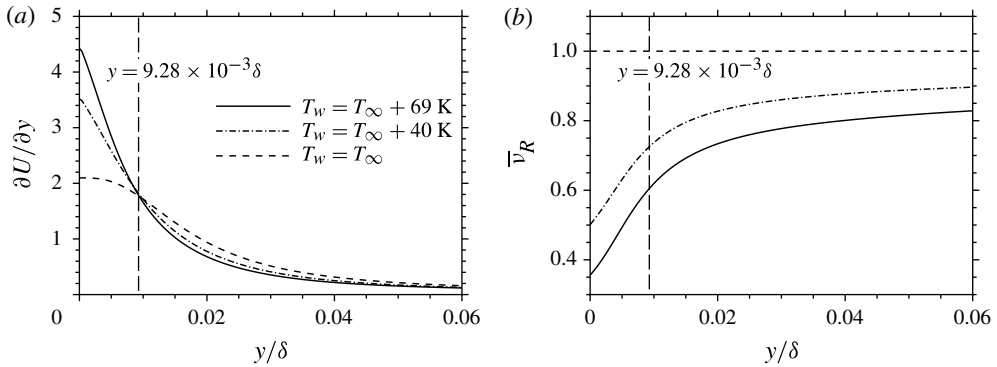

FIGURE 8. Wall-normal distribution of (*a*) mean-shear rate and (*b*) viscosity ratio at $Re_\theta^{eff} = 1840$.

3.3. *The velocity profile and the thin-layer effects*

In the context of linear theory, the presence of an inflection point in the velocity profile can lead to inviscid instability. Wall & Wilson (1997) referred to this change as the velocity-profile shape effect. In fully turbulent flows, the mean velocity profile is important in determining the turbulence production. The mean-shear rate dU/dy of the near-wall region is shown in figure 8(*a*), normalized by U_∞ and θ_{in}. In the SH case, the shear rate at the wall is increased and reaches twice the magnitude of the reference UH case. However, the difference in the velocity profiles is mostly confined to the near-wall region (see figure 5*a*). The mean-shear rate for SH decreases rapidly away from the wall and becomes smaller than those in the UH and MH cases at $y/\delta > 0.0093$. This location corresponds to the edge of the viscous sublayer based on the UH case, but is inside the buffer region based on both the MH and SH cases. In the region $y/\delta > 0.0093$, although the differences in the shear rates are reduced, the heated velocity profiles exhibit relatively weaker shear.

On the other hand, a thin layer of lower-viscosity fluid near the wall can be regarded as a lubricant, which is the so-called thin-layer effect. Strictly speaking, it is hard to designate the present flow as in the thin-layer category, since the term implies the

presence of an interface between two or more immiscible liquids (Wall & Wilson 1997). If the thin layer is defined as the location where $\partial U/\partial y$ is larger than that of the unheated case, the thickness of the thin layer is approximately $y/\delta = 0.0093$. Figure 8(*b*) shows the mean kinematic viscosity ratio $\bar{\nu}_R$. At the edge of the thin layer, the ratio still remains approximately 72 % (MH) and 60 % (SH). Hence, in the case of wall heating, similarity can be found with the case of a low-viscosity film near the wall. The mean-shear rate is also considerably increased within the thin layer. It is therefore expected that the thin-layer effect will yield the most pronounced contribution to the changes in the skin friction, relative to the bulk and velocity profile effects.

The above results support the view that, among the three physical mechanisms put forward by Wall & Wilson (1997), the thin-layer effect is probably the most prominent in the current flow. The low viscosity of the near-wall region in the case of heating can result in decreased skin friction as if a low-viscosity film were applied on the wall.

The results presented in this section raise two principal questions: first, what is the cause of the reduced turbulence intensity in the region $y/\delta > 0.015$ and enhanced turbulence activity for $y/\delta < 0.015$? Second, what is the main contributing factor to the reduction in C_f? The above two questions are addressed in §§ 4 and 5 respectively.

4. Turbulence budget

4.1. *Turbulent kinetic energy budget*

Statistical analysis of DNS data yields all the terms in the budget for the turbulent kinetic energy (TKE) explicitly. Such an analysis can therefore clarify the dynamical characteristics of turbulence, for example the production, redistribution and dissipation of TKE. Since the viscosity is not constant in the momentum equation, additional terms related to the viscosity gradient and fluctuations must be evaluated. The TKE equation for temperature-dependent viscosity is:

$$\frac{\partial}{\partial t}\left(\frac{1}{2}\overline{u_i'u_i'}\right) + C = P + \Pi + G + T + D + \epsilon$$
$$+ D^{VS1} + D^{VS2} + D^{VS3} + D^{VS4} + \epsilon^{VS1} + \epsilon^{VS2}, \qquad (4.1)$$

where

$$C = U_j\frac{\partial}{\partial x_j}\left(\frac{1}{2}\overline{u_i'u_i'}\right), \quad P = -\overline{u_i'u_j'}\frac{\partial U_i}{\partial x_j} \qquad (4.2a,b)$$

$$\Pi = \overline{p'\frac{\partial u_i'}{\partial x_i}}, \quad G = -\frac{\partial}{\partial x_i}\left(\overline{p'u_i'}\right) \qquad (4.2c,d)$$

$$T = -\frac{\partial}{\partial x_j}\left(\frac{1}{2}\overline{u_i'u_i'u_j'}\right), \quad D = \frac{\bar{\nu}_R}{Re_{\theta_{in}}}\frac{\partial^2}{\partial x_j^2}\left(\frac{1}{2}\overline{u_i'u_i'}\right) \qquad (4.2e,f)$$

$$\epsilon = -\frac{\bar{\nu}_R}{Re_{\theta_{in}}}\overline{\frac{\partial u_i'}{\partial x_j}\frac{\partial u_i'}{\partial x_j}}, \qquad (4.2g)$$

$$D^{VS1} = \frac{2}{Re_{\theta_{in}}}\frac{\partial}{\partial x_j}\left(\overline{\nu_R'u_i'}S_{ij}\right), \quad D^{VS2} = \frac{2}{Re_{\theta_{in}}}\frac{\partial}{\partial x_j}\left(\overline{\nu_R'u_i's_{ij}}\right) \qquad (4.2h,i)$$

$$D^{VS3} = \frac{1}{Re_{\theta_{in}}}\frac{\partial\bar{\nu}_R}{\partial x_j}\frac{\partial}{\partial x_j}\left(\frac{1}{2}\overline{u_i'u_i'}\right), \quad D^{VS4} = \frac{1}{Re_{\theta_{in}}}\frac{\partial\bar{\nu}_R}{\partial x_j}\frac{\partial}{\partial x_i}\left(\overline{u_i'u_j'}\right) \qquad (4.2j,k)$$

$$\epsilon^{VS1} = -\frac{2}{Re_{\theta_{in}}} \overline{\nu'_R \frac{\partial u'_i}{\partial x_j} s_{ij}}, \quad \epsilon^{VS2} = -\frac{2}{Re_{\theta_{in}}} \overline{\nu'_R \frac{\partial u'_i}{\partial x_j} S_{ij}}. \quad (4.2l,m)$$

The terms in the transport equation are: C is convection by the mean flow, P is production, $\Pi + G$ is the velocity–pressure-gradient correlation, T is turbulent transport, D is viscous diffusion due to mean viscosity, ϵ is dissipation, $S_{ij} = (\partial U_i/\partial x_j + \partial U_j/\partial x_i)/2$ and $s_{ij} = (\partial u'_i/\partial x_j + \partial u'_j/\partial x_i)/2$. We have herein decomposed the viscous diffusion and dissipation terms into the contributions due to the effective viscosity, D and ϵ respectively, and all other contributions due to viscosity stratification. The latter terms are marked by superscript 'VS'. This choice is in contrast to the work of Zonta *et al.* (2012) where all the viscous diffusion terms were lumped together. Here, D^{VS1} and D^{VS2} are related to viscosity–velocity correlation, and D^{VS3} and D^{VS4} are related to mean viscosity gradient. Furthermore, ϵ^{VS1} and ϵ^{VS2} are related to viscosity–velocity-gradient correlation. The budget for the TKE, $k = (u_i u_i)/2$, is shown in figure 9, normalized by U_∞^3/θ_{in}, where VS denotes the sum of all the additional terms which arise due to the viscosity variation, i.e. $VS = D^{VS1} + D^{VS2} + D^{VS3} + D^{VS4} + \epsilon^{VS1} + \epsilon^{VS2}$. Statistical convergence was verified by ensuring that $(\partial/\partial t)(\overline{u'_i u'_i}/2)$ was two orders of magnitude smaller than the leading terms in the budget.

In the case of wall heating, the peak value of the production is reduced and its wall-normal position also decreases. In particular, $P = 9.17 \times 10^{-4}$ and 7.77×10^{-4} for the UH and SH cases, respectively, and these peak values correspond to $y_v^+ = 11.0$ and 9.72 (or $y/\delta = 0.0181$ and 0.0115). Since both the mean-shear rate and Reynolds shear stress in the buffer region are reduced for the heated wall, the reduced production is inevitable.

Despite the decrease in the mean viscosity near the wall, the magnitude of the dissipation term is increased in the case of wall heating. It is evident from figure 9 that the magnitude of ϵ is rather significantly increased for the heated wall. While viscous diffusion is balanced by the dissipation at the wall for the UH case, in the heated flow the dissipation balances the sum of viscous diffusion and the additional VS terms. Above the viscous sublayer ($y_v^+ > 5$), the dissipation term of the heated flow becomes smaller than that of the unheated case.

Since the magnitudes of the dissipation and the production are most dominant relative to the other terms within the viscous sublayer and in the buffer layer, respectively, the kinetic energy produced in the buffer layer is transported to the sublayer to maintain the energy balance (Pope 2000). The larger dissipation of the heated flow causes the energy transfer to become more pronounced, relative to the unheated case. As a result, figure 9(b) shows enhanced viscous diffusion in addition to the newly derived additional VS terms. The VS term is the second largest gain in the viscous sublayer. Furthermore, the VS term is negative (loss) near the production peak and is positive (gain) in the sublayer. Even though the VS terms involve both diffusion-like and dissipation-like elements, their overall contribution is energy transfer, i.e. receiving energy at the peak production and releasing energy in the sublayer. Therefore, the VS terms transport TKE toward the wall similarly to viscous diffusion due to the effective viscosity.

All the terms related to viscosity stratification (marked with superscript *VS* in (4.1)) are shown in figure 10. These terms are appreciable only beneath the buffer layer, where the viscosity varies sharply. In the sublayer, D^{VS1}, D^{VS2} and D^{VS3} are positive, i.e. gain terms, while ϵ^{VS1} and ϵ^{VS2} are negative, i.e. loss terms; D^{VS4} is negligible throughout the entire flow. The first two elements, D^{VS1} and D^{VS2} which are related to viscosity-velocity correlation, have negative peaks at the buffer region and positive
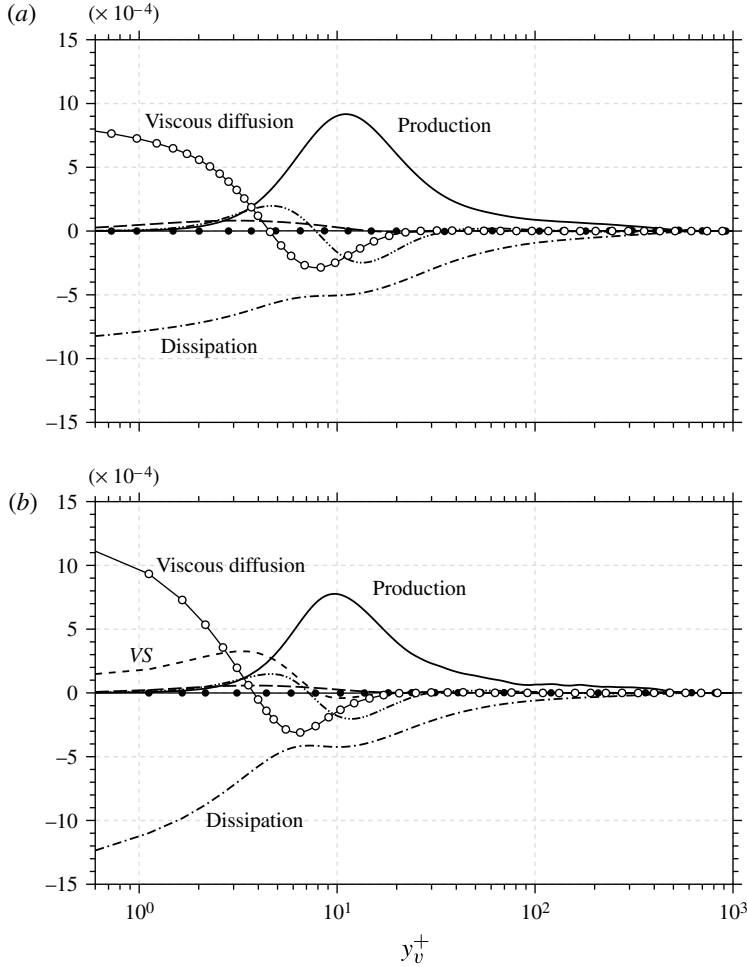
FIGURE 9. Budgets of turbulent kinetic energy for (*a*) $T_w = T_\infty$ (UH) and (*b*) $T_w = T_\infty + 69$ K (SH) at $Re_\theta^{eff} = 1840$. Every term is normalized by U_∞^3/θ_{in}. ——, production; – · · –, dissipation; – – –, sum of the VS terms ($D^{VS1} + D^{VS2} + D^{VS3} + D^{VS4} + \epsilon^{VS1} + \epsilon^{VS2}$); — —, pressure diffusion; – – – –, turbulent transport; —●—, convection; —○—, viscous diffusion.

peaks in the sublayer. This is a similar behaviour to the viscous diffusion, and can be interpreted as an energy transfer mechanism towards the wall. However, D^{VS3} only has a positive peak inside the sublayer. Thus, even though the formulation of D^{VS3} is a viscous-diffusion-like term, it is indeed regarded as production near the wall due to the mean viscosity gradient. The additional dissipation terms (ϵ^{VS1} and ϵ^{VS2}) are negative inside the sublayer, but much smaller than D^{VS3}. Therefore, this result suggests that wall heating on the present fluid would enhance the TKE near the wall. A simple explanation can be given in terms of the local Reynolds number, here defined as $Re_\theta(x, y) \equiv U_\infty \theta(x)/\nu(y)$. Wall heating leads to larger $Re_\theta(x, y)$ at a given height within the thermal boundary layer due to the lower viscosity near the heated wall. As a result, the TKE is enhanced in the near-wall region.
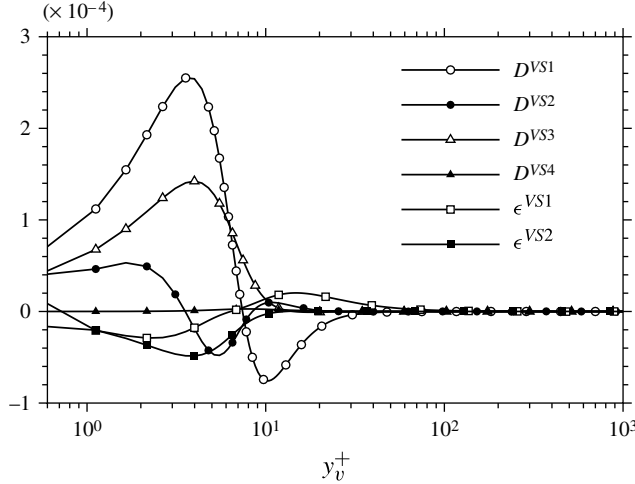
FIGURE 10. Wall-normal profile of the additional VS terms in the turbulent kinetic energy budget for $T_w = T_\infty + 69$ K (SH). Each term is normalized by U_∞^3/θ_{in}.

The turbulent kinetic energy budget highlights an interesting observation regarding the dissipation. Despite the lower effective viscosity, the dissipation is increased in the viscous sublayer in contrast to other drag-reduced flows (Choi *et al.* 1994; Min *et al.* 2003; Ricco *et al.* 2012). This trend is explained in §4.2 by considering the fine-scale turbulent motion.

4.2. *Fine-scale motion: dissipation*

Examination of the TKE budget indicated that the dissipation is enhanced when the flow is heated. In this subsection, the origin of the larger dissipation is investigated. The premultiplied energy spectra of the streamwise velocity fluctuations $k_z \Phi_{u'u'}(\lambda_z)$ are shown in figure 11(*a*) in order to evaluate the most energetic spanwise wavelength and its wall-normal location. The spectrum $k_z \Phi_{u'u'}(\lambda_z)$ is given by

$$k_z \Phi_{u'u'}(\lambda_z) = k_z \int_{-\infty}^{\infty} \overline{u'(z)u'(z+\zeta)} \mathrm{e}^{-\mathrm{i}k_z\zeta} \mathrm{d}\zeta, \tag{4.3}$$

where k_z is the spanwise wavenumber. When the flow is heated, the energy in the small wavelengths increases near the wall. Since the dissipation range corresponds to short wavelengths, less than 60η (Pope 2000), the increased energy of short wavelengths near the wall is consistent with the augmented dissipation. Remarkably, the spectra show decreased energy at relatively large wavelength in the outer region. This result indicates that wall heating intensifies the turbulent motion of the fine scales near the wall, and weakens that of the large scales in the outer region. Figure 11(*b*) shows contours of the difference in the spectra between the strongly heated and the unheated cases, defined as $k_z \Phi_{u'u'}(\lambda_z)|_{SH} - k_z \Phi_{u'u'}(\lambda_z)|_{UH}$. It is clear that the energy spectral density of the heated wall is increased near the wall and decreased in the outer region. When the log-scale is taken into account, it is apparent that the wall-normal range of decrease in energy is larger than that of increase in energy. The negative peak is located at approximately $y/\delta \approx 0.055$ with wavelength $\lambda_z/\delta \approx 0.25$. The positive peak is located near $y/\delta \approx 0.006$ with $\lambda_z/\delta \approx 0.13$. This supports the conclusion that
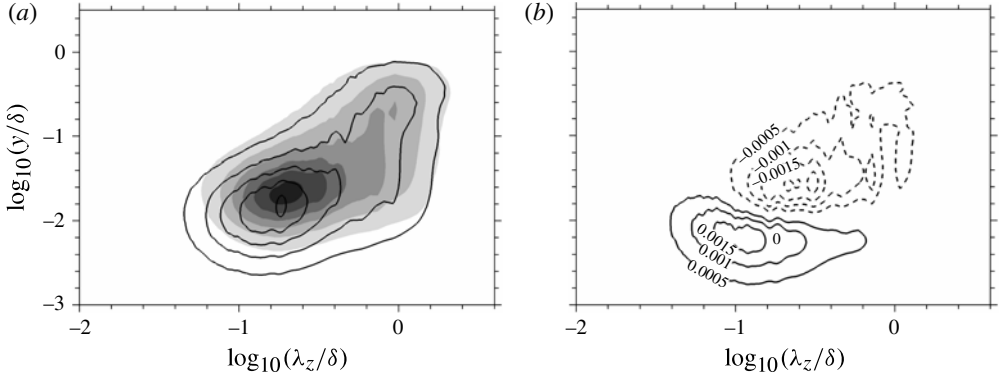
FIGURE 11. (*a*) One-dimensional premultiplied energy spectra $k_z \Phi_{u'u'}(\lambda_z)$ at $Re_\theta^{eff} = 1840$ for (solid lines) the strongly heated wall and (grey contours) the unheated wall. The contour levels start at 0.001 with increment of 0.001, normalized by θ_{in} and U_∞. (*b*) Difference in the spectra between the SH and the UH cases defined as $k_z \Phi_{u'u'}(\lambda_z)|_{SH} - k_z \Phi_{u'u'}(\lambda_z)|_{UH}$.
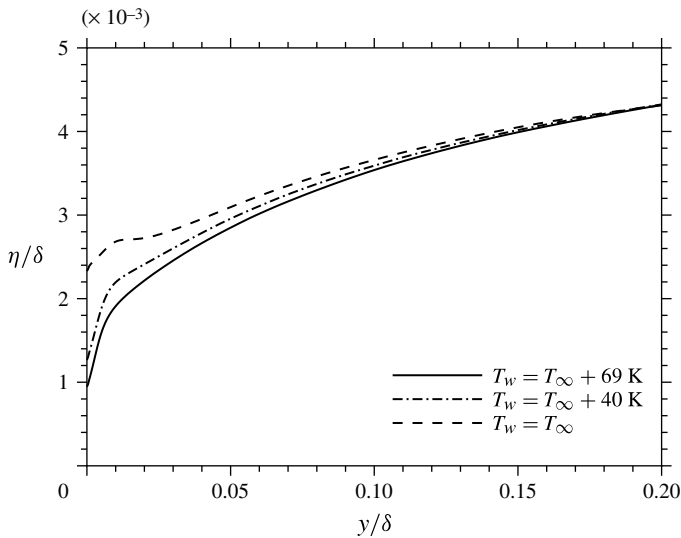

FIGURE 12. Kolmogorov microscale at $Re_\theta^{eff} = 1840$.

the excess in kinetic energy in the buffer layer (figure 5*b*) is transported towards the wall and not towards the outer region. The findings of the energy spectra are in agreement with the behaviour of the Kolmogorov microscale (see figure 12). The length scale demonstrates that the smallest eddy size depends on the change of the fluid temperature. In particular, the Kolmogorov length is significantly decreased near the hot wall. Since the dissipation range is approximately proportional to the size of the smallest eddies (Pope 2000), it is inferred that the increased dissipation near the heated wall results from the reduction in the size of the smallest eddies in this region.

The enhanced dissipation can be examined by considering topological characteristics of the local rate-of-strain tensor, $S_{ij} = (\partial u_i / \partial x_j + \partial u_j / \partial x_i)/2$. For incompressible flows,
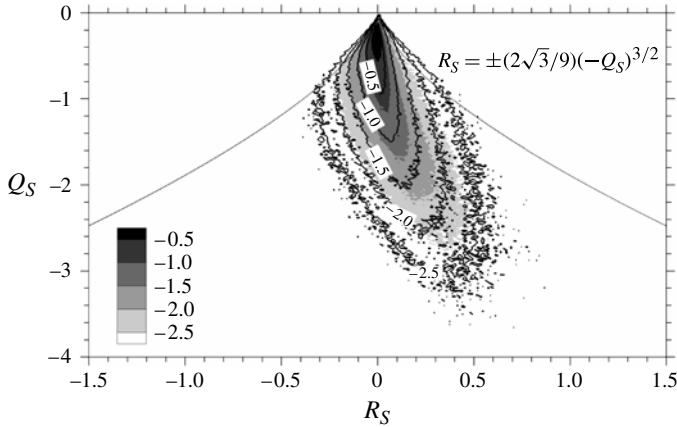
FIGURE 13. Joint p.d.f. plots of Q_S versus R_S at $y/\theta_{in} = 0.110$ ($y^+ = 5.5$ for the unheated case). Line isocontours are for the strongly heated wall, and grey contours correspond to the unheated flow. The plots show half-decade contours of relative frequency. Velocity gradients have been normalized by U_∞/θ_{in}.

the first invariant is identically zero, and the remaining two are $Q_S \equiv -(S_{ij}S_{ji})/2$ and $R_S \equiv -(S_{ij}S_{jk}S_{ki})/3$, respectively (Blackburn, Mansour & Cantwell 1996; Ooi *et al.* 1999). The invariant Q_S is proportional to the negative of the kinetic energy dissipation (Soria *et al.* 1994). Thus large negative values of Q_S point to enhanced rates of kinetic energy dissipation. Figure 13 shows contours of the joint probability density functions (p.d.f.s) of the invariants in the viscous sublayer. The spatial extent of each contour is enlarged for the heated flow. The area within a contour level is dependent on the Reynolds number (Soria *et al.* 1994). The reduction in local viscosity near the heated wall leads to an increase in the local Reynolds number and, as a result, expands the contours of the Q–R joint p.d.f. Since the large region of Q_S is a site of high dissipation, this result is consistent with the TKE budget which indicated increased dissipation near the hot wall. Moreover, at the same physical wall-normal location, the contours of the joint p.d.f. are aligned more closely with the vertical axis in the case of the heated flow. This reflects that the influence of the wall, where the contours collapse onto a vertical line, is further extended to higher wall-normal positions. All the above results provide compelling evidence of enhanced dissipation in the presence of wall heating due to intensified fine-scale motion.

The primary conclusion drawn from the turbulence budget is that the production is reduced by the wall heating, and the dissipation is increased due to the enhanced fine-scale motion in the heated flow. The investigation of the turbulence budget clearly explains the changes in the turbulence activity questioned in the previous section. Lower production of kinetic energy is tightly related to the Reynolds shear stress, $\overline{u'v'}$. In the next section, a detailed view of the contribution of the Reynolds shear stress to C_f is sought by investigating the detailed flow structure.

5. Skin friction and vortical structures

5.1. *Skin-friction coefficient*

It is well known that C_f is related to the growth rate of the momentum thickness (White 2006). As shown in figure 7(*a*), wall heating leads to a decrease in the

growth rate of θ, which is accompanied by a reduction in the skin-friction coefficient. Inspection of contributions to C_f is required in order to elucidate the skin-friction reduction mechanism. These contributions are analysed using a modification of the identity by Fukagata, Iwamoto & Kasagi (2002) (referred to herein as FIK). The FIK identity is computed from the triple integration of the Reynolds-averaged Navier–Stokes (RANS) equations for the streamwise momentum in the wall-normal direction, and it provides a detailed view of the various contributions to C_f. For the present flow, the FIK identity is modified as follows in order to take into account the viscosity variation:

$$
C_{f,FIK} = \underbrace{\frac{4}{\delta^2 Re_{\theta_{in}}} \int_0^\delta \bar{\nu}_R U \, \mathrm{d}y}_{C_f(U)} - \underbrace{\frac{4}{\delta^2} \int_0^\delta (\delta - y) UV \, \mathrm{d}y}_{C_f(UV)} - \underbrace{\frac{4}{\delta^2} \int_0^\delta (\delta - y)\overline{u'v'} \, \mathrm{d}y}_{C_f(u'v')}
$$

$$
\underbrace{- \frac{4}{\delta^2 Re_{\theta_{in}}} \int_0^\delta (\delta - y) \left(U \frac{\partial \bar{\nu}_R}{\partial y} \right) \mathrm{d}y}_{C_f(U\bar{\nu}_y)} + \underbrace{\frac{4}{\delta^2 Re_{\theta_{in}}} \int_0^\delta (\delta - y) \left(\overline{\nu'_R \frac{\partial u'}{\partial y}} \right) \mathrm{d}y}_{C_f(\nu'u'_y)}
$$

$$
+ \underbrace{\frac{2}{\delta^2 Re_{\theta_{in}}} \int_0^\delta (\delta - y)^2 \frac{\partial}{\partial x} \left(\bar{\nu}_R \frac{\partial U}{\partial x} \right) \mathrm{d}y}_{C_f(\bar{\nu}U_x)}
$$

$$
+ \underbrace{\frac{2}{\delta^2 Re_{\theta_{in}}} \int_0^\delta (\delta - y)^2 \frac{\partial}{\partial x} \left(\overline{\nu'_R \frac{\partial u'}{\partial x}} \right) \mathrm{d}y}_{C_f(\nu'u'_x)}
$$

$$
\underbrace{- \frac{2}{\delta^2} \int_0^\delta (\delta - y)^2 \frac{\partial}{\partial x} (UU) \, \mathrm{d}y}_{C_f(UU)} - \underbrace{\frac{2}{\delta^2} \int_0^\delta (\delta - y)^2 \frac{\partial}{\partial x} \left(\overline{u'u'} \right) \mathrm{d}y}_{C_f(u'u')}
$$

$$
\underbrace{- \frac{2}{\delta^2} \int_0^\delta (\delta - y)^2 \left(\frac{\partial P}{\partial x} \right) \mathrm{d}y}_{C_f(P)}. \tag{5.1}
$$

The above equation demonstrates that C_f comprises the effect of the mean and the turbulent motions as well as the effect of the variable local viscosity. Similarly to the governing equations, the above expression for C_f is normalized by the momentum thickness at the inlet and the free-stream velocity. Equation (5.1) shows that C_f is dependent not only on the near-wall dynamics (Kravchenko, Choi & Moin 1993; Choi *et al.* 1994), but also the outer flow via a filter $(\delta - y)$.

Figure 14 shows the skin-friction coefficient obtained from the FIK identity, $C_{f,FIK}$, as a function of Re_θ^{eff}. $C_{f,FIK}$ with the viscosity variation is in good agreement with the results obtained directly from statistical averaging of the wall-shear stress in the DNS, and reproduces the decrease in skin friction in the heated flows as previously shown in figure 3(*a*).

Figure 15 displays the various contributions to C_f in the FIK identity for the SH and the UH cases. These contributions can be sorted in terms of relative magnitude in the following order: the Reynolds shear stress $C_f(u'v')$, the streamwise gradient of the
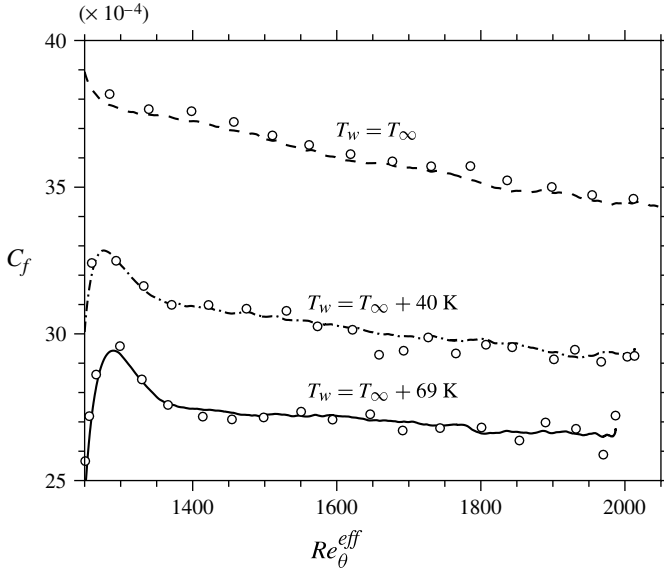
FIGURE 14. Skin-friction coefficients, computed from the wall shear stress C_f (lines) and from the FIK identity $C_{f,FIK}$ (symbols) as a function of the effective Reynolds number.
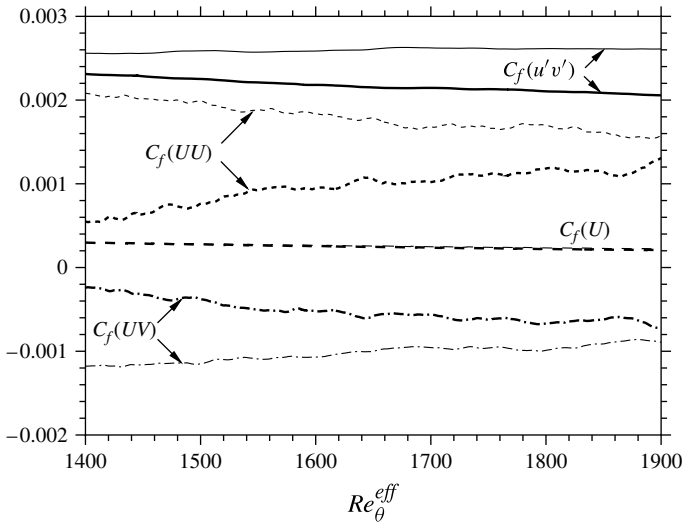

FIGURE 15. Contributions to the skin-friction coefficient. Thick and thin lines indicate $T_w = T_\infty + 69$ K (SH) and $T_w = T_\infty$ (UH), respectively.

squared mean streamwise velocity $C_f(UU)$, the product of the mean streamwise and wall-normal velocities $C_f(UV)$ and the product of the mean viscosity and streamwise velocity $C_f(U)$. The contribution of these terms is dependent on the effective Reynolds number. Remaining terms in the modified FIK identity are negligible, of order 10^{-5}, and are not shown. In the presence of wall heating, $C_f(u'v')$ and $C_f(UU)$ contribute

to the reduction of the skin friction, while $C_f(UV)$ has an opposite effect, which favours an increase in the total friction. The term $C_f(U)$ is insensitive to wall heating. Although the viscosity ratio itself does not contribute significantly, both the mean and turbulent flow fields with the altered viscosity ratio cause the reduction in C_f.

The term $C_f(UU)$ is reduced due to the changes in the mean flow in the thin near-wall thermal layer. In this layer, the velocity profile is fuller in the heated flow and spreads at a relatively slower rate due to the lower viscosity. The magnitude of the term $C_f(UV)$ is reduced due to a decrease in the mean vertical velocity in the heated flow, which is consistent with the reduction in the displacement thickness δ^* (figure 7a). The difference in $C_f(u'v')$ between the heated and unheated flows becomes larger as the Reynolds number is increased. However, differences in $C_f(UU)$ and $C_f(UV)$ diminish downstream. That is, for high Reynolds number, the contribution of $C_f(u'v')$ to the reduction of skin friction becomes relatively more important.

It is evident from figure 15 that $C_f(u'v')$ is the most important turbulence contribution to the reduction of the skin friction. This observation motivates a close investigation of the Reynolds shear stress across the heated boundary layer. A discussion in terms of turbulent structures is presented in the next subsection.

5.2. *Reynolds shear stress: sweeps and ejections*

Quadrant analysis of the Reynolds shear stress identifies the main contributions to turbulence production, and provides an interpretation of these contributions in terms of flow events (Willmarth & Lu 1972; Brodkey, Wallace & Eckelmann 1974). The analysis divides the Reynolds shear stress into four categories according to the sign of u' and v'. The first quadrant Q1 ($u' > 0$ and $v' > 0$) contains outward motion of high-speed fluid; the second quadrant Q2 ($u' < 0$ and $v' > 0$) contains outward motion of low-speed fluid referred to as ejection events; the third quadrant Q3 ($u' < 0$ and $v' < 0$) contains inward motion of low-speed fluid; and the fourth quadrant Q4 ($u' > 0$ and $v' < 0$) contains an in-rush of high-speed fluid referred to as sweep events. Here, Q1 and Q3 events contribute to the positive Reynolds shear stress (negative production), and Q2 and Q4 events contribute to the negative Reynolds shear stress (positive production). Figure 16 shows the contributions from each quadrant plotted as a function of the wall-normal coordinate. In the case of wall heating, all contributions to the Reynolds shear stress are attenuated with similar proportions. Owing to their large magnitude, the Q2 and Q4 stresses show the largest reduction in absolute terms. Reduction in Q2 and Q4 events has previously been reported in drag-reduced flows (Choi *et al.* 1994). Even though the contributions of the negative Reynolds shear stress (Q1 and Q3) are somewhat decreased (an increase in C_f in (5.1)), the relatively more pronounced reduction in the positive shear stresses can lead to an overall decrease of the skin-friction coefficient (see (5.1)). It should be remarked that the results in figure 16 are normalized by the free-stream reference speed, in order to demonstrate the effect of heating relative to the isothermal flow. On the other hand, the contribution of each quadrant would be nearly unchanged when normalized by the respective $-\overline{u'v'}$ from each case.

In addition to the streamwise and wall-normal velocity fluctuations, the influence of viscosity fluctuations is also considered in terms of contribution to the Reynolds shear stress. The octant analysis for the Reynolds shear stress is presented in figure 17. Only the heated cases ($T_w = T_\infty + 40$ K and $T_w = T_\infty + 69$ K) are shown. Both Q1
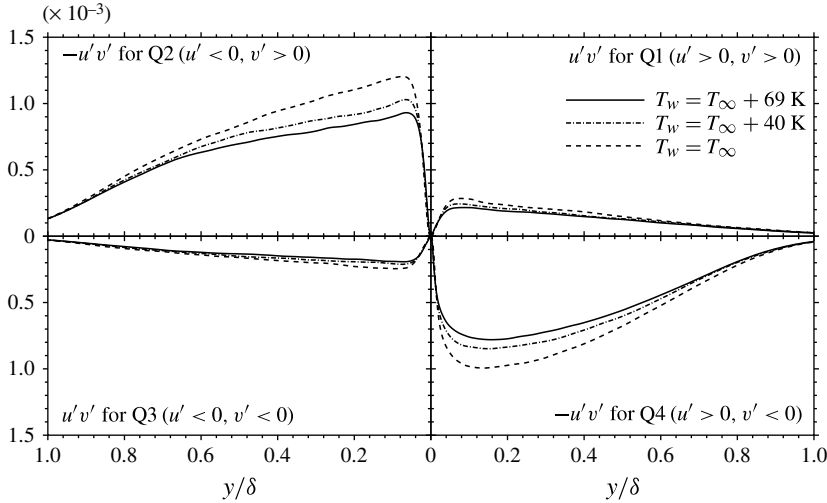
FIGURE 16. Contributions to the Reynolds shear stress $(-\overline{u'v'})$ from each quadrant at $Re_\theta^{eff} = 1840$. Each profile is normalized by the free-stream velocity.
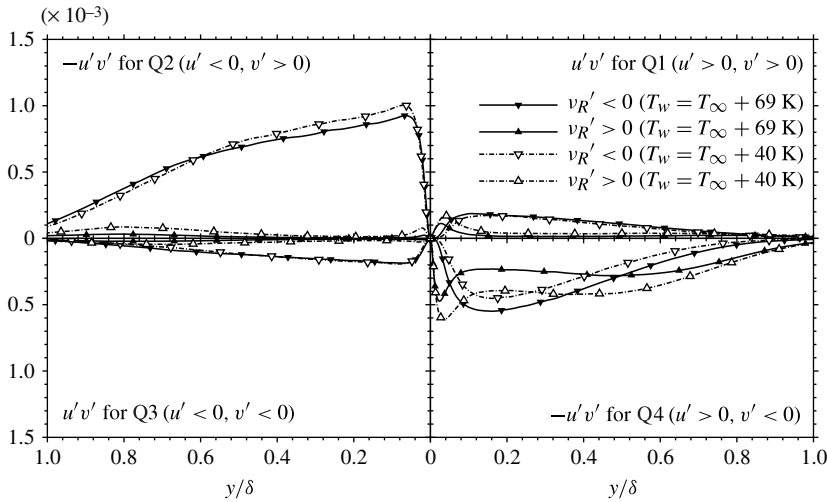

FIGURE 17. Octant analysis of the Reynolds shear stress $(-\overline{u'v'})$ at $Re_\theta^{eff} = 1840$. Each profile is normalized by the free-stream velocity.

and Q3 events are dominated by low-viscosity (hot fluid) events. However, they remain inappreciably affected by heating. Attention is focused instead on Q2 and Q4 events.

Since a lower-viscosity fluid is established near the hot wall, it is conceivable that ejection events are mostly associated with the upwards displacement of low-viscosity (hot) fluid. This is illustrated in figure 17 where Q2 events consist predominantly of the contribution due to low-viscosity (hot) fluid motion. In the case of Q4 events, contributions of both high- and low-viscosity fluid appear important. The former are intuitive, and can be attributed to sweeps of outer fluid ($y/\delta > 0.5$ for the SH case).
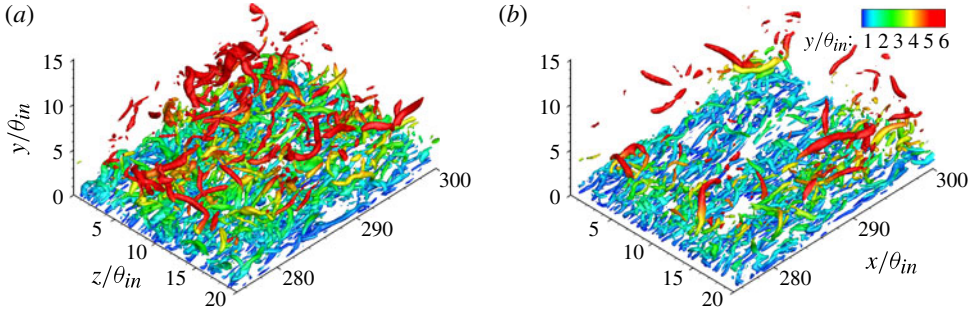
FIGURE 18. Isosurfaces of vortical structures using $\lambda_2 \theta_{in}^2/U_\infty^2 = -0.03$. (*a*) $T_w = T_\infty$ (UH) and (*b*) $T_w = T_\infty + 69$ K (SH). Colour indicates wall-normal location of the isosurface.

On the other hand, the displacement of low-viscosity fluid towards the heated surface must be carefully interpreted. These events are identified as $\nu'_R < 0$ relative to the mean, or effective, viscosity which is a smooth function in the wall-normal coordinate. Therefore, they represent sweeps of instantaneously hotter fluid than the mean. The net effect of wall heating on Q4 events is an overall reduction in the contribution to Reynolds stress, as shown in figure 16. Previous studies (Adrian, Meinhart & Tomkins 2000; Lee & Sung 2009) have shown that Q4 events are observed adjacent to the heads of hairpin vortices, or the spanwise vortices. The current results therefore motivate an investigation of the strength of the spanwise vortices, and whether they are weakened for the heated wall – a point that we address in the next subsection.

5.3. *Outer vortical structures*

For the heated flow, the TKE budget exhibited a reduction in the peak value of production in the buffer region. Furthermore, the energy spectra demonstrated that TKE in the buffer and outer regions was reduced across all scales. Thus, it can be inferred that turbulent motions are weakened in those regions in response to heating. Moreover, it is necessary to understand the effect of the turbulence structures in the outer region on the skin friction. In this subsection, we discuss the weakened vortical structures in the outer region due to wall heating.

In order to distinguish the vortical structures, a vortex identification method based on λ_2 is adopted. Here, λ_2 is defined as the second largest eigenvalue of the tensor $S_{ik}S_{kj} + \Omega_{ik}\Omega_{kj}$, where S_{ij} is the symmetric component and Ω_{ij} is the antisymmetric component of the velocity gradient tensor (Jeong & Hussain 1995). The instantaneous three-dimensional vortical structures are visualized in figure 18, which shows that the outer vortical structures ($y/\theta_{in} > 2$) become sparse for the higher wall temperature. This result is in agreement with Zonta *et al.* (2012), who showed a reduction in the population of vortices near the hot wall of turbulent channel flow. However, in the current work, the structures close to the wall (blue isosurfaces) remain unaffected. In order to compare the strength of the outer vortical structures, the p.d.f. of $\lambda_{2,neg}$ at $y/\delta = 0.1$ and 0.4 is shown in figure 19. Here, $\lambda_{2,neg}$ is defined as $-\lambda_{2,neg}$ for $\lambda_2 < 0$ and zero for $\lambda_2 > 0$. At $y/\delta = 0.1$ (figure 19*a*) for the heated flows, although the probability of $\lambda_{2,neg} < 0.015$ (weak vortical motion) is increased, there is a rather significant reduction in the probability of $\lambda_{2,neg} > 0.015$ (strong vortical motion). The same observation is valid at $y/\delta = 0.4$ (figure 19*b*), e.g. increased probability of $\lambda_{2,neg} < 0.006$ and decreased probability of $\lambda_{2,neg} > 0.006$ for heated flows. This
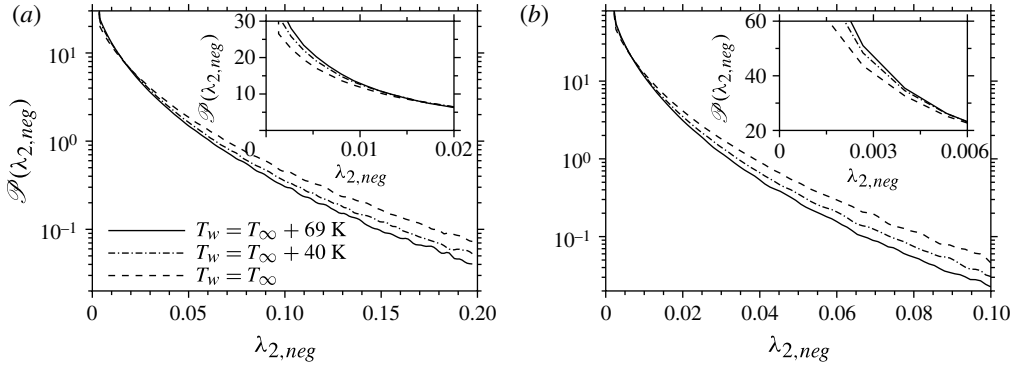
FIGURE 19. p.d.f. of $\lambda_{2,neg}$, $\mathscr{P}(\lambda_{2,neg})$, at (*a*) $y/\delta = 0.1$ and (*b*) $y/\delta = 0.4$.

statistically supports the observations from instantaneous fields (e.g. figure 18) which show a decrease in the population of the outer vortical structures for the heated flow. The changes in the vortical structures is consistent with the reduced turbulence intensity (figure 5*b*), since vortical structures are closely related to the production of Reynolds shear stress (Robinson 1991). It should be noted that the weakened vortices have been found in various drag-reduced wall-bounded flows including the work of Choi *et al.* (1994) and Kim *et al.* (2007). It is also important to remark that the majority of the difference is observed in the outer region. Thus, the population of spanwise vortices, which reside in that region, is substantially reduced. The less frequent occurrence of outer vortices results in decreased Q2 and Q4 events in the outer region as shown in figure 16.

Instantaneous realizations such as figure 18 provide empirical evidence that the turbulence activity is reduced in the outer flow, in accord with the change in TKE. A primary statistical corroboration is provided by figure 19, and further confirmation is sought for the changes in the outer flow structures. Conditionally averaged vortical structures can be evaluated using a linear stochastic estimation (LSE) based on the velocity vector that makes the largest contribution to the Reynolds shear stress (Moin, Adrian & Kim 1987). In order to determine the conditional event vector $(u', v') = (u'_m, v'_m)$, the maximum values of the probability-weighted Reynolds shear stress $u'v'\mathscr{P}(u', v')$ are extracted (see the inset of figure 20*a*). The angle and strength of the vectors are shown in figure 20. This result demonstrates that the angle of the event vector with the largest contribution to the Reynolds shear stress is similar for all cases with and without heating. The magnitudes of both the streamwise and the wall-normal components are only slightly decreased for the heated case.

Isosurfaces of λ_2 are displayed in figure 21. The vortex identification criterion is evaluated from the stochastically estimated velocity field of the Q2 event defined by $\langle u'_i(x')|u'_m(x), v'_m(x)\rangle$. Note that λ_2 is normalized by U_∞ and θ_{in} which are identical among all cases. Therefore, any changes in λ_2 can be interpreted as variations in the size of the structures in the heated flows relative to the unheated case. In the region $0.1 < y/\delta < 0.4$, the conditional structures which yield Q2 events are hairpin-like in shape: they have a spanwise-vortex head with counter-rotating pairs of streamwise vortices. Both the inclination angle of the legs and the spanwise spacing between the centres of the streamwise vortex pair are insensitive to the wall temperature and the associated viscosity variation. However, the streamwise lengths of the vortices
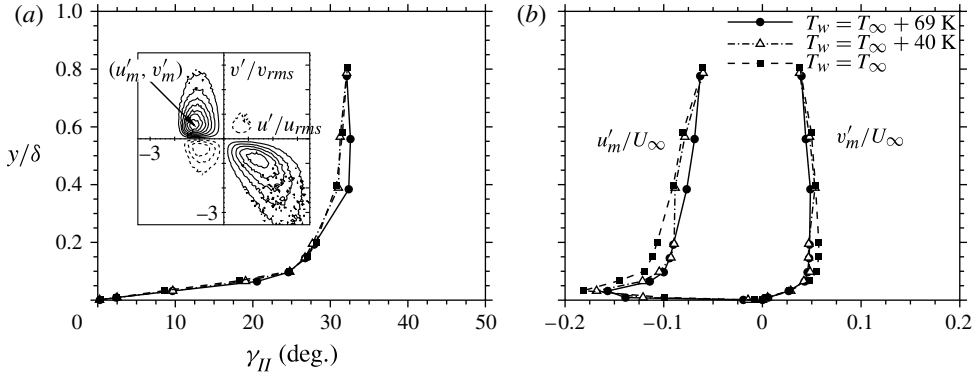
FIGURE 20. (a) Angle of the velocity vector ($\gamma_{II} = \tan^{-1}(v'_m/u'_m)$) with the maximum contribution to the Q2 component of the Reynolds shear stress. The inset shows an example of contours of probability-weighted Reynolds shear stress $u'v'\mathscr{P}(u', v')$ at $y^+ = 5.5$ for the unheated case. (b) The conditional event vectors u'_m and v'_m are normalized by U_∞.
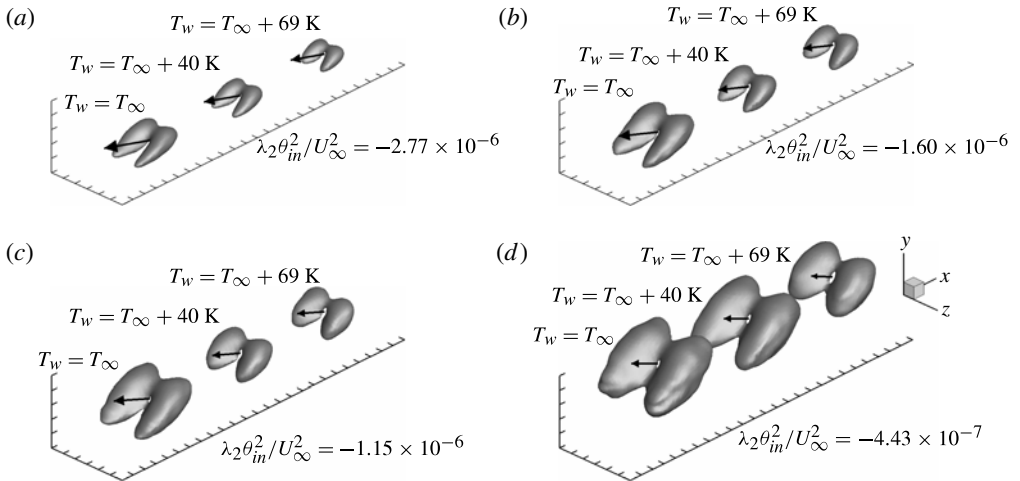

FIGURE 21. Vortical structures of the linearly estimated flow field with the Q2 event $(u', v', w') = (u'_m, v'_m, 0)$ at $Re_\theta^{eff} = 1840$: (a) $y/\delta = 0.1$; (b) $y/\delta = 0.15$; (c) $y/\delta = 0.2$; (d) $y/\delta = 0.4$. The vortices are identified with an isosurface of λ_2 (15 % of the minimum λ_2 of UH case). The vectors represent the velocity events used in the estimation. The distance between ticks on each axis is $1\theta_{in}$.

decrease with increasing wall temperature. For example, the streamwise extents of the eddies for the SH case are decreased by approximately 25 % and 15 % from those of UH flow at $y/\delta = 0.1$ and 0.4, respectively. Together with the observation from figure 19, this result implies that the swirling motion of the individual vortex located in the outer region of the SH flow is weaker than that of the UH case. This result, and the observations from instantaneous realizations of outer vortices (e.g. figure 18) and the findings from the quadrant analysis (figure 16), are all clear evidence that the weakened Q2 events in the heated flow lead to decreased C_f due to a reduced contribution from the Reynolds shear stress. It should be noted that, if the local
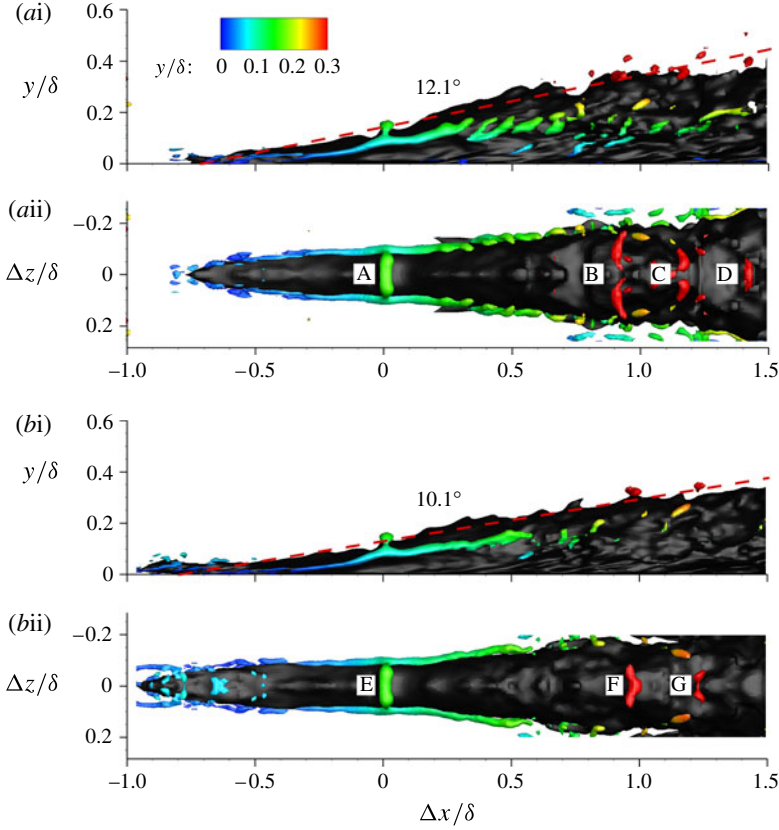
FIGURE 22. Linearly estimated velocity field for a spanwise vortex at $y/\delta = 0.15$ for (*a*) $T_w = T_\infty$ (UH) and (*b*) $T_w = T_\infty + 69$ K (SH) at $Re_\theta^{eff} = 1840$; (i) side view; and (ii) top view. The vortices are identified with an isosurface of λ_2 ($\lambda_2\theta_{in}^2/U_\infty^2 = -2.5$). Colour indicates wall-normal location of the isosurface. The volume of negative streamwise velocity is identified with a black isosurface of $u'/\sqrt{u'^2 + v'^2 + w'^2} = -0.8$.

friction velocity is used for normalization ($\lambda_2\theta_{in}^2/u_\tau^2$), the size of the structures in figure 21 shows a weaker dependence on temperature. However, the objective of the figure is to demonstrate the decrease in the absolute size of the vortical structure, for the heated cases relative to the isothermal condition. For the purpose of such comparison, U_∞ and θ_{in} are the appropriate reference scales for normalization.

A stochastic estimation of the conditionally averaged velocity fields around the single spanwise vortex $\langle u_i'(x')|\lambda_{2z,neg}(x)\rangle$ at $y_{ref}/\delta = 0.15$ is illustrated in figure 22. Here, $\lambda_{2z,neg}$ is defined as $-\lambda_{2z}$ for $\lambda_{2z} < 0$ and zero for $\lambda_{2z} > 0$. Note that each velocity vector in the estimated flow fields is normalized to unity in order to clearly show weak motions away from the event locations (Christensen & Adrian 2001). It can be seen that the head of a hairpin-like vortex (spanwise vortex) is located at the reference location. Spanwise vortices are observed downstream of the event location, and have the appearance of a packet enclosing low-speed fluid. The downstream vortices are located further away from the wall as compared with the event location, due to the inclination angle of the shear layer (or the hairpin packet).

The streamwise spacing of the spanwise vortices and inclination angle of the packet are estimated from the top and side views in figure 22, respectively. The angle of the inclined shear layer (figure 22ai, bi), which is a junction of ejection and sweep motion, is decreased for the strongly heated flow. Originally the vortical motions are inclined away from the wall at an angle of 12.1° (shown by the dashed red line). However, the angle is reduced to 10.1° for the heated flow. The decreased inclination angle of the shear layer, which is a typical characteristic of accelerated boundary layers (Dixit & Ramesh 2010), is consistent with the fuller mean-velocity profile in the strongly heated flow (figure 5). Furthermore, figure 22($a$ii,$b$ii) demonstrates that the streamwise spacing of the spanwise vortices is increased for $T_w = T_\infty + 69$ K. Two distinct swirling patterns (position marked 'F' and 'G') are evident downstream of the event location for $T_w = T_\infty + 69$ K, whereas three (position marked 'B', 'C' and 'D') are visible for $T_w = T_\infty$. Streamwise coherence of the hairpins produces stronger backflow of u' (Adrian $et\ al.$ 2000). Thus, it could be inferred that the strength of low-speed velocity perturbation (black isosurface) is weakened for the heated flow owing to the decreased streamwise succession of spanwise vortices. Since the low-speed fluid inside the vortex packet is formed by multiple Q2 events in turbulent bursts, it is expected that the magnitude of the Reynolds shear stress for the heated wall is decreased and thus the contribution of the Reynolds shear stress to the skin-friction coefficient is also reduced.

6. Summary and conclusions

DNS of turbulent boundary layers with temperature-dependent viscosity were performed to investigate the influence of wall heating on skin friction. The fluid viscosity model was chosen to represent water at atmospheric pressure. Based on the free-stream temperature of 30°C, two wall temperatures (70°C and 99°C) were considered. These wall temperatures correspond to viscosity ratios (ν_R) of approximately half and 35 % at the wall. A simulation without wall heating was also performed for comparison. When the wall is heated, viscosity is decreased within the momentum boundary layer owing to the high Prandtl number. The skin-friction reduction was evaluated and changes in the turbulent flow fields due to the present flow configuration were examined. The skin-friction reduction mechanism was discussed with focus on turbulent structures and their role.

The skin-friction coefficient can be reduced by up to 26 % of its reference value within the simulated Reynolds number range. Profiles of velocity and scalar fields were presented scaled by the modified inner length scale for the inhomogeneous viscosity. The log-law of the mean streamwise velocity profile was shifted upward, similarly to previous drag-reduced flows. The turbulence intensity and the Reynolds shear stress were decreased in the heated flows. In addition, both the mean scalar and scalar fluctuation of the present flows were reduced relative to the constant-viscosity configuration. The DNS results were examined in terms of the three physical effects proposed by Wall & Wilson (1997). There was no significant bulk effect, or changes in the outer velocity profile. However, the thin-layer effect caused an appreciable change in the turbulence statistics.

The budget of the turbulent kinetic energy demonstrated that the production term was weakened in the heated flow, owing to the weaker Reynolds shear stress. On the other hand, the near-wall dissipation was increased despite the lower viscosity near the wall. The enhanced dissipation was described by the premultiplied energy spectra and the joint p.d.f. of Q_S and R_S, which showed augmented near-wall fine-scale motion. In addition, terms due to viscosity stratification were shown to have an effect

similar to viscous diffusion. It was concluded that viscosity stratification leads to larger energy transfer towards the wall from the buffer region, compared to the flow over the unheated wall.

Next, the skin-friction reduction mechanism was investigated. In order to quantify various contributions to the skin-friction coefficient, the FIK identify by Fukagata *et al.* (2002) was extended to the case of viscosity-stratified TBLs. The present study revealed that the skin-friction reduction by wall heating was mainly due to the slower downstream development of U^2 and the reduced Reynolds shear stress. To support the findings based on the FIK identity, the origin of decreased Reynolds shear stress was demonstrated. Quadrant and octant analysis showed that Q2 and Q4 events of the Reynolds shear stress were significantly reduced in the outer region over the heated walls. Finally, the weakening of the outer vortical structures by flow heating was demonstrated by LSE of the ejection events and spanwise vortices.

A scenario is proposed for the mechanism of skin-friction reduction by wall heating. First, when the wall is heated, the viscosity inside the thermal boundary layer is decreased. Here, the thermal boundary layer is thinner than the momentum counterpart due to relatively high Prandtl number for liquids. This results in slower streamwise growth of the momentum deficit in the near-wall region for the heated cases, and it is evident that $\partial(UU)/\partial x$ in this layer is decreased. Since the contribution of this term to the skin friction decays quadratically away from the wall, the near-wall behaviour prevails and the skin friction is reduced. In addition, the turbulence activity and kinetic energy are reduced due to a combined effect of enhanced dissipation and weakened production. The former is caused by the enlarged dissipation range in the near-wall region. The reduction in production is due to the decrease in intensity of vortical structures in the outer region, and in turn a decrease in the Reynolds shear stress. The Reynolds shear stress is also the largest contributor to the skin-friction coefficient. Therefore, the skin-friction coefficient is inevitably reduced by the combined effect of reduced Reynolds shear stress and the weaker variation in the mean momentum near the wall.

The current results provide clear evidence that wall heating yields skin-friction reduction. The underlying mechanism is of theoretical and practical importance. The present analysis focused on viscosity stratification in zero-pressure-gradient boundary layers, while all other thermal properties were constant. Future work should therefore include the effects of buoyancy, thermal diffusivity and pressure gradients.

Acknowledgements

REFERENCES

ADRIAN, R. J., MEINHART, C. D. & TOMKINS, C. D. 2000 Vortex organization in the outer region of the turbulent boundary layer. *J. Fluid Mech.* **422**, 1–54.

BLACKBURN, H. M., MANSOUR, N. N. & CANTWELL, B. J. 1996 Topology of fine-scale motions in turbulent channel flow. *J. Fluid Mech.* **310**, 269–292.

BRODKEY, R. S., WALLACE, J. M. & ECKELMANN, H 1974 Some properties of truncated turbulence signals in bounded shear flows. *J. Fluid Mech.* **63**, 209–224.

BUSHNELL, D. M. & MOORE, K. J. 1991 Drag reduction in nature. *Annu. Rev. Fluid Mech.* **23**, 65–79.

CECCIO, S. L. 2010 Friction drag reduction of external flows with bubble and gas injection. *Annu. Rev. Fluid Mech.* **42**, 183–203.

CHOI, H., MOIN, P. & KIM, J. 1993 Direct numerical simulation of turbulent flow over riblets. *J. Fluid Mech.* **255**, 503–539.

CHOI, H., MOIN, P. & KIM, J. 1994 Active turbulence control for drag reduction in wall-bounded flows. *J. Fluid Mech.* **262**, 75–110.

CHRISTENSEN, K. T. & ADRIAN, R. J. 2001 Statistical evidence of hairpin vortex packets in wall turbulence. *J. Fluid Mech.* **431**, 433–443.

DIXIT, S. A. & RAMESH, O. N. 2010 Large-scale structures in turbulent and reverse-transitional sink flow boundary layers. *J. Fluid Mech.* **649**, 233–273.

FUKAGATA, K., IWAMOTO, K. & KASAGI, N. 2002 Contribution of Reynolds stress distribution to the skin friction in wall-bounded flows. *Phys. Fluids* **14**, L73–L76.

HUANG, P. G., COLEMAN, G. N. & BRADSHAW, P. 1995 Compressible turbulent channel flows: DNS results and modelling. *J. Fluid Mech.* **305**, 185–218.

INCROPERA, F. P. & DEWITT, D. P. 1985 *Fundamentals of Heat and Mass Transfer*. John Wiley and Sons.

JACOBS, R. G. & DURBIN, P. A. 2001 Simulations of bypass transition. *J. Fluid Mech.* **428**, 185–212.

JEONG, J. & HUSSAIN, F. 1995 On the identification of a vortex. *J. Fluid Mech.* **285**, 69–94.

KADER, B. A. 1981 Temperature and concentration profiles in fully-turbulent boundary layers. *Intl J. Heat Mass Transfer* **24**, 1541–1544.

KAWAMURA, H., OHSAKA, K., ABE, H. & YAMAMOTO, K. 1998 DNS of turbulent heat transfer in channel flow with low to medium-high Prandtl number fluid. *Intl J. Heat Fluid Flow* **19**, 482–491.

KIM, K., LI, C.-F., SURESHKUMAR, R., BALACHANDAR, S. & ADRIAN, R. J. 2007 Effects of polymer stresses on eddy structures in drag-reduced turbulent channel flow. *J. Fluid Mech.* **584**, 281–299.

KONG, H., CHOI, H. & LEE, J. S. 2000 Direct numerical simulation of turbulent thermal boundary layers. *Phys. Fluids* **12**, 2555–2568.

KRAL, L. D. & FASEL, H. F. 1994 Direct numerical simulation of passive control of three-dimensional phenomena in boundary-layer transition using wall heating. *J. Fluid Mech.* **264**, 213–254.

KRAVCHENKO, A. G., CHOI, H. & MOIN, P. 1993 On the relation of nearwall streamwise vortices to wall skin friction in turbulent boundary layers. *Phys. Fluids* A **5**, 3307–3309.

LAUCHLE, G. C. & GURNEY, G. B. 1984 Laminar boundary-layer transition on a heated underwater body. *J. Fluid Mech.* **144**, 79–101.

LEE, J.-H. & SUNG, H. J. 2009 Structures in turbulent boundary layers subjected to adverse pressure gradients. *J. Fluid Mech.* **639**, 101–131.

LI, Q. 2011 Direct and large-eddy simulations of turbulent boundary layers with heat transfer. PhD thesis, Royal Institute of Technology (KTH), Stockholm, Sweden.

MARUSIC, I., MCKEON, B. J., MONKEWITZ, P. A., NAGIB, H. M. & SMITS, A. J. 2010 Wall-bounded turbulent flows at high Reynolds numbers: recent advances and key issues. *Phys. Fluids* **22**, 065103.

MIN, T. & KIM, J. 2004 Effects of hydrophobic surface on skin-friction drag. *Phys. Fluids* **16**, L55–L58.

MIN, T., YOO, J. Y., CHOI, H. & JOSEPH, D. D. 2003 Drag reduction by polymer additives in a turbulent channel flow. *J. Fluid Mech.* **486**, 213–238.

MOIN, P., ADRIAN, R. J. & KIM, J. 1987 Stochastic estimation of organized structures in turbulent channel flow. In Proceedings of 6th Symposium on Turbulent Shear Flows, Toulouse, France, pp. 16.9.1–16.9.8.

NAGIB, H. M. & CHAUHAN, K. A. 2008 Variations of von Kármán coefficient in canonical flows. *Phys. Fluids* **20**, 101518.

NOURGALIEV, R. R. & THEOFANOUS, T. G. 2007 High-fidelity interface tracking in compressible flows: unlimited anchored adaptive level set. *J. Comput. Phys.* **224**, 836–866.

OOI, A., MARTIN, J., SORIA, J. & CHONG, M. S. 1999 A study of the evolution and characteristics of the invariants of the velocity-gradient tensor in isotropic turbulence. *J. Fluid Mech.* **381**, 141–174.

POPE, S. B. 2000 *Turbulent Flows*. Cambridge University Press.

PURTELL, L. P., KLEBANOFF, P. S. & BUCKLEY, F. T. 1981 Turbulent boundary layer at low Reynolds number. *Phys. Fluids* **24**, 802–811.

RICCO, P., OTTONELLI, C., HASEGAWA, Y. & QUADRIO, M. 2012 Changes in turbulent dissipation in a channel flow with oscillating walls. *J. Fluid Mech.* **700**, 77–104.

ROBINSON, S. K. 1991 Coherent motions in the turbulent boundary layer. *Annu. Rev. Fluid Mech.* **23**, 601–639.

ROSENFELD, M., KWAK, D. & VINOKUR, M. 1991 A fractional step solution method for the unsteady incompressible Navier–Stokes equations in generalized coordinate systems. *J. Comput. Phys.* **94**, 102–137.

SAMEEN, A. & GOVINDARAJAN, R. 2007 The effect of wall heating on instability of channel flow. *J. Fluid Mech.* **577**, 417–442.

SCHLATTER, P. & ÖRLÜ, R. 2010 Assessment of direct numerical simulation data of turbulent boundary layers. *J. Fluid Mech.* **659**, 116–126.

SMITS, A. J., MATHESON, N. & JOUBERT, P. N. 1983 Low-Reynolds-number turbulent boundary layers in zero and favourable pressure gradients. *J. Ship Res.* **27**, 147–157.

SORIA, J., SONDERGAARD, R., CANTWELL, B. J., CHONG, M. S. & PERRY, A. E. 1994 A study of the fine-scale motions of incompressible time-developing mixing layers. *Phys. Fluids* **6**, 871–884.

TISELJ, I., POGREBNYAK, E., LI, C., MOSYAK, A. & HETSRONI, G. 2001 Effect of wall boundary condition on scalar transfer in a fully developed turbulent flume. *Phys. Fluids* **13**, 1028–1039.

WALL, D. P. & WILSON, S. K. 1996 The linear stability of channel flow of fluid with temperature-dependent viscosity. *J. Fluid Mech.* **323**, 107–132.

WALL, D. P. & WILSON, S. K. 1997 The linear stability of flat-plate boundary-layer flow of fluid with temperature-dependent viscosity. *Phys. Fluids* **9**, 2885–2898.

WHITE, F. M. 2006 *Viscous Fluid Flow*, 3rd edn. McGraw-Hill.

WILLMARTH, W. W. & LU, S. S. 1972 Structure of the Reynolds stress near the wall. *J. Fluid Mech.* **55**, 65–92.

WU, X. & MOIN, P. 2010 Transitional and turbulent boundary layer with heat transfer. *Phys. Fluids* **22**, 085105.

ZAKI, T. A., WISSINK, J. G., RODI, W. & DURBIN, P. A. 2010 Direct numerical simulations of transition in a compressor cascade: the influence of free stream turbulence. *J. Fluid Mech.* **665**, 57–98.

ZONTA, F., MARCHIOLI, C. & SOLDATI, A. 2012 Modulation of turbulence in forced convection by temperature-dependent viscosity. *J. Fluid Mech.* **697**, 150–174.